IMM 379
NYO-1480-132
December 1969

Courant Institute of
Mathematical Sciences

Axisymmetric Buckling of Hollow Spheres and Hemispheres

Louis Bauer, Edward L. Reiss, and Herbert B. Keller

Prepared under Contract AT(30-1)-1480
with the U.S. Atomic Energy Commission
and Contract N00014-67-A-0467-0008 with
the office of Naval Research NR 064-438

New York University

NR 064-438

IMM 379
NYO-1480-132
December 1969

New York University

Courant Institute of Mathematical Sciences

AXISYMMETRIC BUCKLING OF HOLLOW SPHERES AND HEMISPHERES

Louis Bauer, Edward L. Reiss, and Herbert B. Keller*

This report represents results obtained at the Courant Institute of Mathematical Sciences, New York University, with the U.S. Atomic Energy Commission, Contract AT(30-1)-1480 and the Office of Naval Research, Contract N00014-67-A-0467-0008. Reproduction in whole or in part is permitted for any purpose of the United States Government.

Distribution of this document is unlimited.

*California Institute of Technology.

ABSTRACT

A nonlinear thin shell theory is derived for the axisymmetric buckling of spherical shells subjected to either a pressure or a centrally directed surface load. The theory is reduced to a boundary value problem for a system of four first order ordinary differential equations. Numerical solutions of this boundary value problem are obtained by the shooting and parallel shooting methods. An extensive numerical study is made of the nonlinear deformations of the shells. We find for example, that all solution branches that bifurcate from the eigenvalues of the linearized buckling theory are connected to each other by means of intermediate branches. Some implications of the numerical results concerning the buckling of spherical shells are discussed.

1. Introduction.

The outer surface of a thin-walled hollow sphere* is subjected to a uniform compressive load p. It may be either a pressure or a centrally directed load. The uniformly contracted spherical shell is a possible equilibrium state for all values of p. This state occurs in experiments only for sufficiently small p. When p increases to or beyond some critical pressure the shell suddenly jumps or buckles with finite displacements into a non-spherical shape.

The classical or linear buckling theory [1] yields an eigenvalue problem with the eigenvalue parameter proportional to p. The spectrum is discrete and the lowest eigenvalue is usually called the buckling load. For sufficiently thin shells the eigenfunction or buckling mode consists of many waves over the surface of the shell with an undetermined amplitude. The experimentally measured buckling loads are frequently considerably less than the lowest eigenvalue. The experimentally observed deformation is usually a "dimple" confined to a neighborhood of one point with the remainder of the shell remaining nearly spherical. Kármán and Tsien [2] suggested that a nonlinear theory is required to adequately describe the buckling of spherical shells. They treated the complete spherical shell as a clamped shallow spherical cap corresponding to the region where the dimple occurs. Their analysis was subsequently refined and generalized in [3,4,5,6,7] and elsewhere.** The solutions

---

* For example, a ping-pong ball.

** We refer to the discussion and the extensive bibliographies in [7,8] for references to previous investigations.

of a nonlinear theory have been analyzed in [8,9,15] by a perturbation methods for loads near the eigenvalues of the linearized theory.

In this paper we consider the nonlinear axisymmetric deformations of the hollow sphere. An appropriate shell theory is derived in Section 2 and in Appendix I. The strain displacement relations and the curvature expressions differ from those employed in [8,9]. The shell theory is reduced to a two point boundary value problem, which we call Problem S, for a system of four first order ordinary differential equations. The boundary value problem is the same for pressure or centrally directed loading. We employ the shooting and parallel shooting methods to obtain extensive numerical solutions of Problem S. The numerical methods are described in Section 4. The results of the computations are presented in Section 5. Their implications concerning buckling are discussed in Section 6.

2. Formulation.

Let r, θ, ϕ denote a spherical coordinate system. The radial distance from the origin is r. The polar angle θ is measured from the north pole, $\theta = 0$, and is in the range $0 \leq \theta \leq \pi$. The circumferential angle ϕ varies in the interval $0 \leq \phi \leq 2\pi$. The inner and outer surfaces of the thin spherical shell are given by $r = R \mp h$ where R is the radius of the midsurface of the shell and $2h$ is the uniform thickness. The shell is deformed by a uniform compressive surface load p.

It is either directed toward the center r = 0 or it is a pressure that is normal to the deformed surface. We show in Appendix I that our shell theory is the same for both loads.

We consider only the axisymmetric deformations of the shell. Thus all displacements and stresses are independent of ϕ. The displacements in the θ and the negative r directions are denoted respectively by $\bar{U}(r,\theta)$ and $\bar{W}(r,\theta)$. The ϕ displacement vanishes because the deformation is axisymmetric. The exact Lagrangian strain displacement relations in spherical coordinates are

$$(2.1a) \qquad e^*_{\theta\theta}(r,\theta) = \frac{(\bar{U}_\theta - \bar{W})}{r}\left[1 + \frac{1}{2}\frac{(\bar{U}_\theta - \bar{W})}{r}\right] + \frac{1}{2}\left[\frac{\bar{U}+\bar{W}_\theta}{r}\right]^2 ,$$

$$(2.1b) \qquad e^*_{\phi\phi}(r,\theta) = \frac{(\bar{U}\cot\theta - \bar{W})}{r}\left[1 + \frac{1}{2}\frac{(\bar{U}\cot\theta - \bar{W})}{r}\right] ,$$

$$(2.1c) \qquad e^*_{r\theta}(r,\theta) = \frac{1}{2}\left[\frac{(\bar{U}+\bar{W}_\theta)}{r}(\bar{W}_r - 1) + \bar{U}_r\left(1 + \frac{\bar{U}_\theta - \bar{W}}{r}\right)\right] .$$

Here the subscripts on e^* signify the components of strain. The subscripts on $\bar{U}$ and $\bar{W}$ denote partial differentiation. The shear strains $e^*_{r\phi}$ and $e^*_{\theta\phi}$ vanish because the deformations are axisymmetric. The strain e^*_r is not included since it is subsequently neglected in deriving the shell theory.

We assume that the displacements are small but finite. Specifically, this means that

$$(2.2) \qquad \frac{|\bar{U}_\theta - \bar{W}|}{r} , \quad \frac{|\bar{U}\cot\theta - \bar{W}|}{r} , \quad |\bar{W}_r| \ll 1 .$$

We use (2.2) in (2.1) and obtain the approximate nonlinear strain displacement relations,

$$(2.3a) \qquad e^*_{\theta\theta} \approx E_\theta(r,\theta) \equiv \frac{\bar{U}_\theta - \bar{W}}{r} + \frac{1}{2}\left(\frac{\bar{U} + \bar{W}_\theta}{r}\right)^2 ,$$

$$(2.3b) \qquad e^*_{\phi\phi} \approx E_\phi(r,\theta) \equiv \frac{\bar{U}\cot\theta - \bar{W}}{r} ,$$

$$(2.3c) \qquad e^*_{r\theta} \approx E_{r\theta}(r,\theta) \equiv \frac{1}{2}\left[\bar{U}_r - \frac{(\bar{U}+\bar{W}_\theta)}{r}\right] .$$

The customary assumptions of shell theory are that: the shell is thin, i.e. $h/r << 1$; normals to the midsurface remain normal to the deformed midsurface; the normal stress in the r direction is negligible compared to the other normal stresses; the absolute values of the strains $<< 1$; the two dimensional Hooke's law is valid. Thus we define a new dependent variable z by

$$(2.4) \qquad z = R - r , \qquad |z| \leq h ,$$

and we assume that

$$(2.5) \qquad \bar{W}(r,\theta) = RW(\theta) , \qquad \bar{U}(r,\theta) = RU(\theta) - zV(\theta) .$$

Here U and W are dimensionless midsurface displacements and V is proportional to the angle of rotation of a tangent to a meridian. Inserting (2.5) in (2.3c) and setting $E_{r\theta} = 0$ on $z = 0$ we obtain

(2.6) $$V = U + W' ,$$

where a prime denotes differentiation with respect to θ.

By substituting (2.4)-(2.6) in (2.3a,b) we obtain, since $|z/R| << 1$,

(2.7) $$E_\theta(z,\theta) = e_\theta(\theta) - z\kappa_\theta(\theta) ,$$
$$E_\phi(z,\theta) = e_\phi(\theta) - z\kappa_\phi(\theta) .$$

Here the midsurface strains, e_θ and e_ϕ, and the curvatures, κ_θ and κ_ϕ, are defined by

(2.8a) $$e_\theta \equiv U' - W + \tfrac{1}{2} V^2 , \quad e_\phi \equiv U \cot \theta - W,$$

(2.8b) $$\kappa_\theta \equiv V'/R , \quad \kappa_\phi \equiv (V/R)\cot \theta .$$

The relations (2.8a) have been previously employed by Friedrichs [4] but the curvature expressions (2.8b) differ from those in [4]. Koiter [8], Thompson [9] and others use (2.8) with V replaced by W'. The strain displacement equations previously used in analyzing spherical caps, see e.g. [10], are obtained from (2.8) by replacing V by W' and cot θ by $1/\theta$.

The shell equilibrium equations and boundary conditions are derived in Appendix I using the principle of minimum potential energy. They are reduced to a boundary value problem for the following system of four first order ordinary differential equations:

(2.9a) $$\underset{\sim}{y}'(\theta) = \underset{\sim}{f}(\underset{\sim}{y},\theta) , \qquad 0 \leq \theta \leq \pi .$$

Here $\underset{\sim}{y}(\theta)$ is a four dimensional vector with components $y_i(\theta)$, $i = 1,2,3,4$ and $\underset{\sim}{f}(\underset{\sim}{y},\theta)$ is the four dimensional vector with components f_i, $i = 1,2,3,4$ defined by

$$
\begin{aligned}
f_1 &\equiv -(1-\nu)y_1 \cot\theta + y_2 + (k\cot^2\theta - P)y_4 + y_2 y_4 \cot\theta \ , \\
f_2 &\equiv y_3 \ , \\
f_3 &\equiv y_2(\cot^2\theta - \nu) - y_3 \cot\theta - y_4 - y_4^2(\cot\theta)/2 \ , \\
f_4 &\equiv (1-\nu^2)y_1/k - \nu y_4 \cot\theta \ .
\end{aligned} \tag{2.9b}
$$

The parameters P and k are defined by

$$
P \equiv 2^{-1}(p/E)(R/2h) \ , \quad k \equiv 3^{-1}(h/R)^2 \ , \tag{2.9c}
$$

where E is Young's modulus and ν is Poisson's ratio. We refer to P as the load. The components of $\underset{\sim}{y}$ are defined in terms of physical quantities by

$$
y_1 = m(\theta), \quad y_2 = q(\theta), \quad y_3 = t(\theta), \quad y_4 = v(\theta) \equiv V \tag{2.10}
$$

where m, q, t are proportional, respectively, to the radial bending moment, the transverse shear, the circumferential membrane stress; see equations (A.2), (A.15c) and (A.18) in Appendix I.

Since the stresses are bounded and the polar axis is a line of symmetry we have the boundary conditions

$$
u = w' = q = 0 \quad \text{at} \quad \theta = 0,\pi \ . \tag{2.11}
$$

Here $u(\theta) \equiv U(\theta)$ and w is defined by

$$
w(\theta) \equiv W(\theta) - W_0 \ , \quad W_0 \equiv (1-\nu)P \ . \tag{2.12}
$$

The quantity W_0 is the radial displacement of the uniformly contracted or unbuckled state. From (2.6), (2.10) and (2.12)

$$v \equiv u + w' \ , \tag{2.13}$$

so that (2.11) and (2.10) imply that

$$y_2 = y_4 = 0 \ , \quad \theta = 0, \pi \ . \tag{2.14}$$

We refer to the boundary value problem (2.9) and (2.14) as Problem S.

If y_1 and y_3 are eliminated from (2.9) we obtain an equivalent system of two second order equations in $y_2 = q$ and $y_4 = v$:

$$Lq + \nu q = - v - (v^2/2) \cot \theta \ , \tag{2.15a}$$

$$Lv - \nu v = [(1-\nu^2)/k][-Pv + q + qv \cot \theta] \ , \tag{2.15b}$$

where the linear differential operator L is defined by

$$Lf \equiv f'' + f' \cot \theta - f \cot^2 \theta \ . \tag{2.15c}$$

The equations of the classical linear theory of bending of spherical shells [11] are obtained from (2.15) by setting $P = 0$ and omitting the nonlinear terms in (2.15a,b). It is not difficult to show that (2.15) or (2.9) reduce to the differential equations of the nonlinear spherical membrane [12] when we formally set $k = 0$. After multiplying (2.15b) by k and setting $k = 0$, the left hand side of (2.15b) formally vanishes if θ is bounded away from 0 and π and the order of the system (2.15)

is reduced. The reduction is not uniform in θ because of the singularity of cot θ at $\theta = 0,\pi$. Thus $\theta = 0,\pi$ are, in some sense, turning points of (2.15) and boundary layers may form at $\theta = 0$ or $\theta = \pi$ (or both) as $k \to 0$. Friedrichs [4], Altshuler [5] and to some extent Gabril'iants and Feodos'ev [6] attempted to analyze this boundary layer.

It is easy to show that if $|u| << |w'|$ and $\theta << 1$ (so that ν is negligible compared to θ^{-2}), (2.15) can be reduced to the spherical cap equations [10].

If $\underset{\sim}{y}^0(\theta)$ is a solution of the hemisphere problem,

$$\underset{\sim}{y}^{0\,\prime} = f(\underset{\sim}{y}^0,\theta) , \qquad 0 \le \theta \le \pi/2 , \tag{2.16a}$$

$$y_2^0 = y_4^0 = 0 \quad , \quad \text{at} \quad \theta = 0 , \pi/2 , \tag{2.16b}$$

then

$$\underset{\sim}{y}(\theta) = \begin{cases} \underset{\sim}{y}^0(\theta) & , \quad 0 \le \theta \le \pi/2 , \\ \underset{\sim}{y}^0(\pi-\theta) & , \quad \pi/2 \le \theta \le \pi , \end{cases} \tag{2.17}$$

is a solution of Problem S. Such a solution, which is symmetric with respect to the equatorial plane, is referred to as a symmetric solution. The hemisphere problem (2.16) is also physically significant. The boundary conditions (2.16b) are consequences of the physical conditions $u(\pi/2) = w'(\pi/2) = q(\pi/2) = 0$. They imply that the edge of the hemisphere cannot rotate or deflect normal to the equatorial plane but it can slide freely tangential to the plane.

We refer to solutions of Problem S which do not satisfy

$\underset{\sim}{y}(\theta) = \underset{\sim}{y}(\pi-\theta)$ as unsymmetric solutions.* If $\underset{\sim}{y}^1(\theta)$ is an unsymmetric solution then another distinct solution is $\underset{\sim}{y}^2(\theta) \equiv \underset{\sim}{y}^1(\pi-\theta)$. The solution $\underset{\sim}{y}^2$ is obtained from $\underset{\sim}{y}^1$ by rotating the sphere so that the north and south poles are interchanged. Thus unsymmetric solutions occur in pairs.

When a solution of Problem S has been obtained u is determined from,**

$$u' - u \cot\theta = (1+\nu)(q \cot\theta - t) - v^2/2 , \tag{2.18}$$

and w from (2.13). Equation (2.18) is singular at $\theta = 0,\pi$. Therefore the boundary conditions $u(0) = 0$ $u(\pi) = 0$ are insufficient to uniquely solve (2.18). Unique solutions of (2.18) are obtained by specifying $u'(0)$ such that $u(\pi/2) = 0$. This is the correct boundary condition for the hemisphere problem. It fixes the rigid body displacement in the complete sphere problem.

The difference between the potential energy of a buckled solution and the unbuckled solution is proportional to

$$e = \int_0^\pi [t^2 + q^2(\cot^2\theta-\nu) + (1-\nu^2)m^2/k + k\nu^2\cot^2\theta - 4Pw]\sin\theta \, d\theta. \tag{2.19}$$

---

*They are unsymmetric with respect to the equator, but still retain their axial symmetry.

**See Appendix I.

3. The Linear Buckling Theory.

The linear buckling theory is obtained by omitting the nonlinear terms $(v^2/2)\cot\theta$ in (2.15a) and $qv\cot\theta$ in (2.15b). The resulting eigenvalue problem has non-zero solutions if and only if

$$(3.1a)\quad P = P_n(k) \equiv [k/(1-\nu^2)][\lambda_n + 1 + \nu] + 1/[\lambda_n + 1 - \nu], \qquad n = 1,2,\ldots ,$$

where

$$(3.1b)\quad \lambda_n \equiv n(n+1) - 2 .$$

The corresponding eigenfunctions are

$$(3.2)\quad q(\theta) = \alpha_n A_n^{(1)}(\theta) , \quad v(\theta) = \beta_n A_n^{(1)}(\theta) ,$$

$$\alpha_n \equiv \beta_n/[\lambda_n+1-\nu] , \qquad n = 1,2,\ldots ,$$

where $\beta_n \neq 0$ are arbitrary constants and $A_n^{(1)}(\theta)$ is the Associated Legendre Function of the first kind of degree n and order 1, [13]. If n is even the corresponding eigenfunction is symmetric with respect to $\theta = \pi/2$ and if P_n is simple, i.e. $P_n \neq P_m$ for any $n \neq m$, it is called a symmetric eigenvalue. If n is odd then the eigenfunction is anti-symmetric and if P_n is simple it is called an unsymmetric eigenvalue. The value of n for which P_n is a minimum depends on k. It may correspond to either a symmetric or an unsymmetric eigenvalue.

The eigenvalues obtained from previous linearized theories [1], differ slightly from (1). For example, the eigenvalues

determined by Zoelly and Schwerin [1] which we denote by P_n' are given by

$$(3.3) \qquad P_n' \equiv \frac{[\lambda_n^2+2\lambda_n+(1+\nu)^2]}{(\lambda_n+1+3\nu)} \left(\frac{k}{1-\nu^2}\right) + (\lambda_n+1+3\nu)^{-1}, \quad n=1,2,\ldots .$$

For n large we obtain from (3.1) and (3.3) that

$$P_n = \lambda_n \frac{k}{1-\nu^2} + \frac{1}{\lambda_n} + (1+\nu) \frac{k}{1-\nu^2} + \ldots$$

$$P_n' = \lambda_n \frac{k}{1-\nu^2} + \frac{1}{\lambda_n} + \left[(1-3\nu) + \frac{9\nu^2+\nu}{\lambda_n}\right] \frac{k}{1-\nu^2} + \ldots .$$

Thus, for large n, P_n is only slightly larger than P_n' since k is small.

In the numerical computations described in the following sections we obtain solutions for a wide range of P values for $k = 10^{-3}$ and $k = 10^{-5}$. In Table I we list, in increasing magnitude, the fifteen lowest eigenvalues computed from (3.1) and (3.3) for these values of k.

For each of these values of k the lowest eigenvalue is unsymmetric. There are other values of k, e.g. $k = 1.2\times10^{-5}$, for which the lowest eigenvalue is symmetric. There are even values of $k = k_{mn} \equiv \frac{1-\nu^2}{(\lambda_n+1-\nu)(\lambda_m+1-\nu)}$ for which the corresponding eigenvalue is a multiple eigenvalue. For example, with $k \doteq .76935\times10^{-3}$, the lowest eigenvalue occurs for $n = 5$ and $n = 6$.

Table IA, $k = 10^{-3}$

n	P_n	P_n'
5	.0675324	.0646786
6	.0706160	.0684843
4	.0750573	.0702911
7	.0799192	.0781080
8	.0936046	.0919527
3	.106244	.0949524
9	.110786	.109220
10	.130993	.129476
11	.153954	.152467
12	.179504	.178037
13	.207540	.206085
2	.219602	.172597
14	.237992	.236545
15	.270812	.269371
16	.305967	.304531

Table IB, $k = 10^{-5}$

n	$P_n \times 100$	$P_n' \times 100$
17	.668365	.665572
16	.671713	.668555
18	.673789	.671270
15	.685593	.681940
19	.686669	.684358
20	.706003	.703853
14	.712402	.708064
21	.731019	.728995
13	.755470	.750161
22	.761113	.759190
23	.795809	.793966
12	.819535	.812815
24	.834726	.832946
25	.877555	.875828
11	.911529	.902695

4. Numerical Methods.

For both the sphere and the hemisphere problems, we must solve (2.9) subject to boundary conditions of the form

$$y_2(0) = y_4(0) = 0 \ , \quad y_2(L) = y_4(L) = 0 \ . \tag{4.1}$$

For the hemisphere $L = \pi/2$ and for the full sphere $L = \pi$. These problems are solved numerically by the shooting method for the hemisphere, and a parallel shooting method for the full sphere. A crucial step is a continuation procedure used to get good estimates of the proper initial data. First we describe our method for the hemisphere problem and then indicate how that procedure is employed to solve the full sphere case. The numerical procedures and the continuation scheme are analyzed rather thoroughly in [14].

4.1 Shooting for Hemispheres.

Consider the initial value problem, with fixed P and k,

$$\underset{\sim}{u}'(\theta) = \underset{\sim}{f}(\underset{\sim}{u},\theta) \ , \tag{4.2a}$$

$$u(0) = \begin{pmatrix} \xi_1 \\ 0 \\ \xi_2 \\ 0 \end{pmatrix} . \tag{4.2b}$$

We denote the solution of (4.2) by $\underset{\sim}{u} = \underset{\sim}{u}(\theta;\xi_1,\xi_2)$. If this solution exists in $0 \leq \theta \leq \pi/2$ for initial parameters ξ_1 and ξ_2 such that

(4.3) $$u_2(\pi/2;\xi_1,\xi_2) = 0 \ , \quad u_4(\pi/2;\xi_1,\xi_2) = 0 \ ,$$

then by (4.1), $\underset{\sim}{y}(\theta) \equiv \underset{\sim}{u}(\theta;\xi_1,\xi_2)$ is a solution of the hemisphere problem. The number of distinct solutions of the hemisphere problem is equal to the number of distinct real roots (ξ_1,ξ_2) of (4.3). These roots are numerically determined using Newton's method, and a continuity procedure. For this purpose we introduce the vectors

(4.4a) $$\underset{\sim}{U}^{(1)}(\theta) \equiv \frac{\partial \underset{\sim}{u}}{\partial \xi_1} \ , \qquad \underset{\sim}{U}^{(2)}(\theta) \equiv \frac{\partial \underset{\sim}{u}}{\partial \xi_2} \ .$$

Then it follows by differentiation in (4.2) that the $\underset{\sim}{U}^{(j)}$ satisfy the linear variational systems:

(4.4b) $$\frac{d\underset{\sim}{U}^{(1)}}{d\theta} = A(\underset{\sim}{u},\theta)\underset{\sim}{U}^{(1)}, \quad \underset{\sim}{U}^{(1)}(0) = \underset{\sim}{e}^{(1)} = \begin{pmatrix} 1 \\ 0 \\ 0 \\ 0 \end{pmatrix};$$

(4.4c) $$\frac{d\underset{\sim}{U}^{(2)}}{d\theta} = A(\underset{\sim}{u},\theta)\underset{\sim}{U}^{(2)}, \quad \underset{\sim}{U}^{(2)}(0) = \underset{\sim}{e}^{(2)} = \begin{pmatrix} 0 \\ 0 \\ 1 \\ 0 \end{pmatrix}.$$

Here A is the fourth order Jacobian matrix,

(4.4d) $$A(\underset{\sim}{u},\theta) \equiv \left(\frac{\partial f_i(\underset{\sim}{u},\theta)}{\partial u_j}\right) \ .$$

Given an initial estimate $(\xi_1^{(0)},\xi_2^{(0)})$ for a root of (4.3), the sequence of Newton iterates $\{\xi_1^{(\nu)},\xi_2^{(\nu)}\}$ is defined by

(4.5a) $$\xi_j^{(\nu+1)} = \xi_j^{(\nu)} + \Delta\xi_j^{(\nu)}; \quad j=1,2; \ \nu=0,1,2\ldots$$

where $(\Delta\xi_1^{(\nu)}, \Delta\xi_2^{(\nu)})$ is the solution of the linear system

(4.5b)
$$U_2^{(1)}(\pi/2)\Delta\xi_1^{(\nu)} + U_2^{(2)}(\pi/2)\Delta\xi_2^{(\nu)} = -u_2(\pi/2;\xi_1^{(\nu)},\xi_2^{(\nu)}) ,$$
$$U_4^{(1)}(\pi/2)\Delta\xi_1^{(\nu)} + U_4^{(2)}(\pi/2)\Delta\xi_2^{(\nu)} = -u_4(\pi/2;\xi_1^{(\nu)},\xi_2^{(\nu)}) .$$

The coefficient elements $U_j^{(i)}(\pi/2)$ in (4.5b) are the corresponding elements in the solution of (4.4) in which $\underset{\sim}{u}(\theta;\xi_1^{(\nu)},\xi_2^{(\nu)})$ is used in the evaluation of $A(\underset{\sim}{u},\theta)$.

A Runge-Kutta method is employed to solve the three initial value problems (4.2), (4.4b) and (4.4c). The singularity at $\theta = 0$ requires special starting procedures. In (4.2a) we simply use the limiting relations

(4.6) $$\underset{\sim}{f}(\underset{\sim}{u}(0), 0) = \begin{pmatrix} 0 \\ \xi_2 \\ 0 \\ \frac{1-\nu}{k}\,\xi_1 \end{pmatrix}$$

obtained from (2.9b) and (4.2) by requiring continuous derivatives at $\theta = 0$. In (4.4b) and (4.4c) the first step in the integration is done with the centered scheme:

(4.7) $$\underset{\sim}{U}(h) = \underset{\sim}{U}(0) + \frac{h}{2}\, A(\tfrac{1}{2}[\underset{\sim}{u}(0) + \underset{\sim}{u}(h)], \tfrac{h}{2})\cdot[\underset{\sim}{U}(0) + \underset{\sim}{U}(h)]$$

where h is the step width. The error is $O(h^3)$ since we use this second order scheme only at one point.

The interval $0 < \theta < \pi/2$ is divided into 100 equal subintervals and the integrations are performed, starting at

$\theta = 0$, over each subinterval with spacings $h_0 = \pi/200$, and $h_1 = h_0/2$. If the maximum relative difference in the two integrations at the end of a subinterval is not less than 10^{-M}, we then halve the step width, and repeat the procedure over the subinterval. When agreement is achieved we proceed to the next subinterval, starting with the original mesh widths h_0 and h_1. The iterates in Newton's method (4.5) are terminated when $\max_{i=1,2} |\Delta\xi_i^{(\nu)}/\xi_i^{(\nu)}| < 10^{-M}$. In most of the calculations $M = 7$. Occasionally a larger value of M is used.

4.2 Continuation Method for Parameter Variation.

After a solution is determined for some value of P with k fixed, (or for some value of k with P fixed) accurate estimates of the initial iterates $\xi_j^{(0)}$ to use for $P \pm \Delta P$ (or for $k \pm \Delta k$) can be obtained by finding $\partial\xi_j/\partial P$ (or $\partial\xi_j/\partial k$). With k fixed let $\xi_j(P)$ denote the exact initial values for any given P. Then the boundary conditions (4.3) yield the identities in P:

$$(4.3') \qquad \begin{aligned} u_2(\pi/2;\xi_1(P),\xi_2(P),P) &= 0 , \\ u_4(\pi/2;\xi_1(P),\xi_2(P),P) &= 0 . \end{aligned}$$

In rewriting (4.3) we have indicated the dependence of $\underset{\sim}{u}$ on P which was previously ignored to simplify the notation. Differentiating each of these identities with respect to P, we obtain, recalling (4.4a),

$$U_2^{(1)}(\pi/2)\dot{\xi}_1(P) + U_2^{(2)}(\pi/2)\dot{\xi}_2(P) = - U_2^{(5)}(\pi/2) ,$$

(4.8)

$$U_4^{(1)}(\pi/2)\dot{\xi}_1(P) + U_4^{(2)}(\pi/2)\dot{\xi}_2(P) = - U_4^{(5)}(\pi/2) ,$$

where we have introduced

(4.9a) $$\underset{\sim}{U}^{(5)}(\theta) \equiv \frac{\partial \underset{\sim}{u}}{\partial P} , \quad \dot{\xi}_i(P) \equiv \frac{\partial \xi_i(P)}{\partial P} , \quad i = 1,2.$$

By differentiating in (4.2) we find with the aid of (2.9b) and (4.4d) that

(4.9b) $$\frac{d\underset{\sim}{U}^{(5)}(\theta)}{d\theta} = A(\underset{\sim}{u},\theta)\underset{\sim}{U}^{(5)} + \begin{bmatrix} -u_4(\theta) \\ 0 \\ 0 \\ 0 \end{bmatrix} , \quad \underset{\sim}{U}^{(5)}(0) = \underset{\sim}{0} .$$

The coefficients in (4.8) are already computed for use in the final Newton iterate (4.5b). Thus only the additional system (4.9b) is solved to evaluate $\dot{\xi}_1$ and $\dot{\xi}_2$ from (4.8). Then for initial estimates we use the first two terms in the Taylor expansion:

(4.10) $$\xi_j^{(0)}(P \pm \Delta P) = \xi_j(P) \pm \dot{\xi}_j(P)\Delta P , \quad j = 1,2.$$

The derivatives $\dot{\xi}_j(P)$ are of physical interest, especially when P is near a bifurcation point or near a local maximum or minimum point of $P(\xi_j)$.

The corresponding continuation analysis and computation for variation of the geometric parameter k follow in an obvious manner. In fact, to replace P by k only the right hand side in (4.8) need by changed by using the components of

(4.11a) $$\underset{\sim}{U}^{(6)}(\theta) \equiv \frac{\partial \underset{\sim}{u}}{\partial k} \quad .$$

Proceeding the same way as in the derivation of (4.9b) we find that

(4.11b) $$\frac{d\underset{\sim}{U}^{(6)}(\theta)}{d\theta} = A(\underset{\sim}{u},\theta)\underset{\sim}{U}^{(6)}(\theta) + \begin{pmatrix} u_4(\theta)\cot^2\theta \\ 0 \\ 0 \\ -\frac{1-\nu^2}{k^2}u_1(\theta) \end{pmatrix}, \quad \underset{\sim}{U}^{(6)}(0) = \underset{\sim}{0}.$$

4.3 Parallel Shooting for the Full Sphere.

We treat the full sphere by employing the previous procedure for two hemispheres.* We integrate from each pole to the equator and adjust four parameters in order to satisfy four continuity conditions at the equator.

Consider the two initial value problems,

*It is inconvenient to treat the full sphere by integrating from $\theta = 0$ and adjusting ξ_1 and ξ_2 to satisfy the two boundary conditions at $\theta = \pi$. Some of the derivatives are indeterminate at $\theta = \pi$, and the derivatives of some of the auxiliary variables $\underset{\sim}{U}^{(1)}$ and $\underset{\sim}{U}^{(2)}$ are infinite there. Numerically, these singularities are handled more readily by the special starting procedure, (4.6) and (4.7), than by integrating up to $\pi-\varepsilon$, and then using special formulas.

$$(4.12a)\qquad \frac{d\underset{\sim}{u}}{d\theta} = \underset{\sim}{f}(\underset{\sim}{u},\theta)\ , \quad \underset{\sim}{u}(0) = \begin{pmatrix} \xi_1 \\ 0 \\ \xi_2 \\ 0 \end{pmatrix}\ , \quad 0 \le \theta \le \pi/2;$$

$$(4.12b)\qquad \frac{d\underset{\sim}{v}}{d\theta} = \underset{\sim}{f}(\underset{\sim}{v},\theta)\ , \quad \underset{\sim}{v}(\pi) = \begin{pmatrix} \xi_3 \\ 0 \\ \xi_4 \\ 0 \end{pmatrix}\ , \quad \pi \ge \theta \ge \pi/2.$$

Here the ξ_i are the four initial parameters, two for each of the two initial value problems. The solutions of these problems are denoted by $\underset{\sim}{u}(\theta;\xi_1,\xi_2)$ and $\underset{\sim}{v}(\theta;\xi_3,\xi_4)$. If we can find ξ_i such that

$$(4.13)\qquad u_j(\pi/2;\xi_1,\xi_2) = v_j(\pi/2;\xi_3,\xi_4)\ , \qquad j = 1,2,3,4,$$

then a solution of the full sphere problem is given by

$$(4.14)\qquad \underset{\sim}{y}(\theta) \equiv \begin{cases} \underset{\sim}{u}(\theta;\xi_1,\xi_2)\ , & 0 \le \theta \le \pi/2, \\ \underset{\sim}{v}(\theta;\xi_3,\xi_4)\ , & \pi/2 \le \theta \le \pi\ . \end{cases}$$

For fixed P and k, the number of distinct solutions of Problem S is equal to the number of distinct real roots $(\xi_1,\xi_2,\xi_3,\xi_4)$ of (4.13).

The equations (4.13) are also solved by Newton's method. Now however there are two nonlinear systems (4.12) and four linear variational systems to be solved for each Newton iteration step. The numerical integration of the initial value

problems is done in the same way as for the hemisphere. All convergence criteria are the same as in the hemisphere calculations. Corresponding continuity methods in both k and P are also used for obtaining initial iterates.

4.4 Parallel Shooting for Hemispheres.

For some of the solution branches for the hemisphere problem boundary layers occur at $\theta = 0$ or $\theta = \pi/2$; see the discussion in Section 5. When a boundary layer occurs at $\theta = \pi/2$ the solution varies rapidly in a small neighborhood of $\theta = \pi/2$. Thus small variations in the parameters ξ_1 and ξ_2 produce large variations in the solution of (4.2) at $\theta = \pi/2$. When a boundary layer occurs at $\theta = 0$, u_2 and u_4 essentially vanish in an interval $a < \theta \leq \pi/2$. Then relatively large changes in ξ_1 and ξ_2 produce small changes in the solution at $\theta = \pi/2$.

In both cases the simple shooting method of Section 4.1 is unsatisfactory for an accurate determination of the roots of (4.3) and parallel shooting is employed. Thus we select a point θ_0 in the interval $0 < \theta_0 < \pi/2$ and integrate from $\theta = 0$ to θ_0 and from $\theta = \pi/2$ to θ_0. The corresponding four initial parameters are determined from continuity requirements analogous to (4.13). The procedure is completely analogous to the parallel shooting for the full sphere described in Section 4.3. Appropriate values of θ_0 are determined from numerical experiments.

5. Presentation of Results.

Extensive numerical solutions of Problem S have been obtained for shells with $k = 10^{-3}$ (the thick sphere) and $k=10^{-5}$ (the thin sphere) over a wide range of P values. For $k=1.2\times10^{-5}$ a less extensive P range has been covered. At the fixed pressure $P = 6\times10^{-4}$ solutions have been obtained for various k in the range $10^{-5} \leq k \leq 2\times10^{-6}$. We shall describe the thick sphere results that seem most relevant to buckling and briefly mention significant differences for the thin sphere case. The implications of these results for axisymmetric buckling are discussed in Section 6.

The thick sphere computations are summarized in Figures 1 and 2 where we plot P vs. A(P) and e(P). The quantity

$$A(P) \equiv \left(\frac{1}{2}\int_0^{\pi} w^2 \, d\theta\right)^{1/2} \geq 0 \tag{5.1}$$

is a measure of the amplitude of the deviation of the deformation at load P from the uniformly compressed state, $w \equiv 0$. Similarly e(P), defined in (2.19), is proportional to the difference between the potential energies of the buckled and unbuckled states at the same load, P. The circles and crosses on the P-axis denote, respectively, the symmetric and unsymmetric eigenvalues of the linear theory (see Table IA in Section 3).

Each point (A(P),P) with $A(P) > 0$ on the graphs in Figure 1 represents buckled states, i.e. nontrivial solutions of Problem S. If the point corresponds to a symmetric state,

then it represents a single solution. If it corresponds to an unsymmetric state, then it represents a pair of solutions. The graphs show that for fixed values of P, Problem S may have many solutions. To describe and discuss this multiplicity, we decompose the graphs of A(P) into single valued segments of maximal extent and denote each such segment by $B_{n,j}$ with integers n and j. The procedure for choosing appropriate values of n and j is described in Section 5.1. This is equivalent to decomposing the graph of e(P) in Figure 2 into monotone segments of maximal extent. The P coordinates of the end points of the segments are denoted by $P^L_{n,j}$ and $P^U_{n,j}$. We call them, respectively, the lower and upper critical points of the segment. If each point on $B_{n,j}$ corresponds to a symmetric [unsymmetric] solution, then we denote the branch of solutions corresponding to $B_{n,j}$ as $B_{n,j}(P)$ $[B^{\pm}_{n,j}(P)]$. The P axis corresponds to the unbuckled states. We shall not include this branch in our discussion of the multiplicity.

Buckled solutions of Problem S are said to <u>bifurcate</u> from the unbuckled solution at or from a pressure P_0 if there is a solution branch, $\underset{\sim}{y}(\theta,P)$ depending continuously on P such that $\underset{\sim}{y}(\theta,P_0) \equiv 0$ and $\underset{\sim}{y}(\theta,P) \neq 0$ for $P \neq P_0$ but $|P-P_0|$ sufficiently small. This solution branch is called a bifurcation branch. The bifurcation branch need not exist for P in a full neighborhood of P_0. If it exists, locally, for $P > P_0$ $(< P_0)$ we say that solutions bifurcate or branch up (down) from P_0.

Our calculations show that there are solutions in a

full neighborhood of each of the symmetric eigenvalues that were analyzed and that solutions branch either up or down from each of the unsymmetric eigenvalues that were analyzed. Furthermore the results indicate that $\phi \equiv (dA(P_n)/dP)^{-1} = 0$ for n odd, i.e. unsymmetric eigenvalues, but not for n even and ϕ is independent of k. These results are in agreement with the conclusions of bifurcation theory [15].

5.1 The Thick Sphere, $k = 10^{-3}$.

Perhaps the most striking observation in the thick sphere case is the fact that all computed branches of solutions, 21 symmetric branches and 16 pairs of unsymmetric branches, are connected. Furthermore, for each branch $B_{n,j}$ the corresponding potential energy $e_{n,j}(P)$ is a monotone decreasing function of P on $P^L_{n,j} \leq P \leq P^U_{n,j}$ (see Figure 2a). All but two of the symmetric branches and five pairs of the unsymmetric branches contained pressures $P = P^E_{n,j}$, called equal energy loads, at which $e_{n,j}(P^E_{n,j})=0$ for a buckled state. The critical pressures, equal energy loads and connectivity of the unsymmetric branches and the first 16 symmetric branches of solutions are summarized in Table II. Each branch bifurcating from an eigenvalue is indicated by an asterisk. This table complements Figures 1 and 2.

The branch $B_{6,1}$ bifurcating up and down from the lowest symmetric eigenvalue $P_6 \doteq 0.7062$ extends from the lower critical load $P^L_{6,1} \doteq .01045$ to the upper critical load $P^U_{6,1} \doteq .07127$. At its lower endpoint $B_{6,1}$ joins the branch we call $B_{6,0}$ whose

Table IIA

Symmetric Branches

Branch $B_{n,j}$	$P^L_{n,j}$	$P^E_{n,j}$ or (P_n)	$P^U_{n,j}$
$B_{6,0}$		.01214	?
	.0104496		
* $B_{6,1}$		(.0706150)	
			.0712660
$B_{6,2}$		.07123	
	.067830[illegible]		
* $B_{4,1}$		(.0750573)	
			.0855778
$B_{4,2}$		.0848	
	.0[illegible]2205		
$B_{4,3}$		---	
			.0662950
$B_{4,4}$		---	
	.04[illegible]22		
* $B_{8,1}$		(.0936046)	
			.109261
$B_{8,2}$		.1077	
	.0656532		
$B_{8,3}$		.1358	
			.1366638
* $B_{10,1}$		(.130993)	
	.0735912		
* $B_{12,1}$		(.179504)	
			.179807
$B_{12,2}$		.1798	
	.105326		
* $B_{2,1}$		(.219602)	
			.306228
$B_{2,2}$		.23797	
	.237956		
* $B_{14,1}$		(.237902)	
			453[illegible]

Table IIB

Unsymmetric Branches

Branch $B^{\pm}_{n,j}$	$P^{L}_{n,j}$	$P^{E}_{n,j}$ or (P_n)	$P^{U}_{n,j}$
* $B_{5,1}$	.0128125	(.0675324)	.0675324
$B_{5,2}$		.0137	.0202242
$B_{5,3}$	.0173426	---	
$B_{5,4}$		---	.0199705
$B_{5,5}$	.0199473	---	
$B_{5,6}$			.0208548
$B_{5,7}$	.0123971 (on $B_{6,1}$)	.01415	
* $B_{7,1}$	.0799192	(.0799192)	.0858161
$B_{7,2}$	.0467240	.0855	
$B_{7,3}$		---	.064663 (on $B_{4,4}$)
* $B_{3,1}$	.106244	(.106244)	.110025
$B_{3,2}$	.105617	.109531	
$B_{3,3}$		---	.105790 (on $B_{8,2}$)
* $B_{9,1}$	.110786	(.110786)	.120483
$B_{9,2}$	.0706469	.118910	
$B_{9,3}$		---	.10349 (on $B_{8,3}$)

lower endpoint is at $P^L_{6,0} = P^L_{6,1}$ and whose upper endpoint has not been determined, but is greater than P = .1; see Figure 1b. At its upper endpoint $B_{6,1}$ joins $B_{6,2}$ whose upper endpoint is at $P^U_{6,2} = P^U_{6,1}$ and whose lower endpoint is at $P^L_{6,2} \doteq .06783$; see Figures 1a and 2a. The labeling of adjacent joining branches follows the arbitrary rule implied above with the proviso that whenver a bifurcation branch occurs, say bifurcating from $P = P_n$, we call it $B_{n,1}$. Thus for example, the branch joining $B_{6,2}$ at its lower critical pressure should be called $B_{6,3}$. But since $B_{6,3}$ bifurcates from P_4 we also call it $B_{4,1}$. The notation in Table II is now rather obvious if we merely observe that most critical pressures, $P^L_{n,j}$ or $P^U_{n,j}$, have dual representations. On the branches bifurcating from unsymmetric eigenvalues the eigenvalues are also upper or lower critical pressures, that is, $P_n = P^L_{n,1}$ or $P_n = P^U_{n,1}$.

In Figures 3 and 4 we show how the solutions for P decreasing on the lowest symmetric bifurcation branch $B_{6,1}$ go over continuously to the solutions for P increasing on the adjacent branch $B_{6,0}$. There is an obvious difference in the shapes and stresses between the states on branches $B_{6,1}$ and $B_{6,0}$ for P > 0.05; compare Figures 3a and 4a with Figures 3c and 4c. However, for P near $P^L_{6,1} = P^L_{6,0} \doteq 0.0105$ the shapes on both branches are quite similar. Thus there is no abrupt change in mode (see Figures 3b and 4b). As P increases the states on $B_{6,0}$ develop a boundary layer near $\theta = \pi/2$. For example, at P = 0.10, $t(\theta)$ is almost constant over $0 \leq \theta \leq \pi/3$ and then

changes rapidly over $\pi/3 < \theta < \pi/2$ to satisfy the boundary conditions. The graph of $w(\theta)$ is approximately a parabola with maximum at $\theta = 0$ so that the deformed sphere is essentially two pushed in hemispheres joined at the equator. The development of the boundary layer and the simple pushed-in shape of the sphere on $B_{6,0}$ suggests that this mode and branch of solutions continue to exist as $P \to +\infty$. The rapid decay of energy $e_{6,0}(P)$ would seem to be consistent with this assumption.

In Figures 5 and 6 we show four solutions on the branches $B_{6,1}$, $B_{6,2}$ and $B_{6,3} \equiv B_{4,1}$. One of these solutions is for $P = .0712594$, near the critical pressure $P^U_{6,1} = P^U_{6,2}$, and another is for $P = .0678672$ near the critical pressure $P^L_{6,2} = P^L_{4,1}$. The other solutions are for P near the bifurcation loads P_6 and P_4. These solutions have distinct mode shapes and relatively small amplitudes since P is close to P_4 or P_6. This behavior is typical for all even n since the solutions on different symmetric bifurcation branches $B_{n,1}$ have distinctly different deformation and stress modes for P near P_n, and as P varies the solutions continuously change on each branch and merge with the solutions on some other branch which is usually not a bifurcation branch.* Thus all symmetric solutions are connected as P varies up and down on the appropriate symmetric branches. The energy variation on all branches is, as previously noted, monotone decreasing. However, for $P < P_2$ the energy on

*The only symmetric bifurcation branches to merge directly with each other were $B_{10,1}$ and $B_{12,1}$.

most symmetric branches is mainly positive but for $P > P_2$ the opposite occurs (the notable exception is $B_{6,0}$, see Figure 2a and Table II).

The pairs of unsymmetric bifurcation branches $B^{\pm}_{n,1}$ merge continuously at the eigenvalues $P = P_n$ for n odd. The branches $B^{\pm}_{5,1}$ bifurcate down from the lowest eigenvalue $P_5 \doteq 0.0675$ and merge, respectively, with $B^{\pm}_{5,2}$ at $P^L_{5,2} \doteq 0.0128$. Similarly, $B^+_{5,2}$ joins $B^+_{5,3}$ which joins $B^+_{5,4}$ which joins $B^+_{5,5}$ which joins $B^+_{5,6}$ which joins $B^+_{5,7}$ which finally joins $B^-_{5,7}$ at $P^L_{5,7} \doteq 0.0124$; see Figure 2b and Table IIB. The obvious mergers also occur for the $B^-_{5,j}$. Since $B^+_{5,7}$ and $B^-_{5,7}$ join at $P^L_{5,7}$ i.e., $\underset{\sim}{y}^+(\theta, P^L_{5,7}) = \underset{\sim}{y}^-(\pi-\theta, P^L_{5,7}) = \underset{\sim}{y}^+(\pi-\theta, P^L_{5,7})$, $B^{\pm}_{5,7}(P)$ must be symmetric at $P = P^L_{5,7}$. Furthermore, the results show that this symmetric state lies on the branch $B_{6,1}$. The value $P^L_{5,7}$ is not a critical pressure for $B_{6,1}$. In fact, we find that $P^L_{6,1} < P^L_{5,7} < P^U_{6,1}$; see Table II. Equal energy loads are found on the branches $B^{\pm}_{5,2}$ and $B^{\pm}_{5,7}$. Graphs of typical solutions on branch $B^{\pm}_{5,1}$ are shown in Figures 7a and 8a. Solutions at some of the upper and lower critical loads $P^U_{5,j}$ and $P^L_{5,j}$ are shown in Figures 7b and 8b. The transition from one branch to another is indicated by these graphs. We note that on $B^+_{5,1}$ the "southern" hemisphere is less distorted than the "northern" hemisphere which suffers a relatively large indentation, or dimple, around the pole. Similar features occur in all the $B^+_{5,j}$ branches.

At each of the unsymmetric eigenvalues P_n, for n = 7,3 and 9 the solutions $B^{\pm}_{n,1}$ bifurcate up and go through a series

of mergers with intermediate branches. Finally, $B^{+}_{n,j}$ joins $B^{-}_{n,j}$ for some j at $P = P^{U}_{n,j}$ or $P = P^{L}_{n,j}$. Again the symmetric state into which the unsymmetric pairs of solutions finally merge is found to lie on some symmetric branch of solutions. For example, $B^{\pm}_{7,3}$ join $B_{4,4}$ at $P^{U}_{7,3} \doteq 0.0646$. Thus we find the amazing result that all bifurcation branches, for both symmetric and unsymmetric modes, are connected to each other by means of intermediate branches. The energies on the bifurcation branches $B^{\pm}_{n,1}$ for n = 7,3,9 are negative for $P > P_n$. They are also negative on $B_{n,2}$ for a limited range of P values.

5.2 The Thin Spheres.

The results for the thin sphere, $k = 10^{-5}$, are summarized in Figures 9 and 10. For this value of k the lowest eigenvalue is also unsymmetric. The eigenvalues for $k = 10^{-5}$ (see Table IB of Section 3), are closely spaced. For example a 10% change in P from $P = P_{17}$ spans seven additional eigenvalues. A 1% change includes two additional eigenvalues. The solutions for the thin sphere are qualitatively similar, in many respects, to those previously discussed for the thick sphere.* All the branches bifurcating from symmetric eigenvalues are continuously connected in the same way as for the thick sphere. The solution branch

*Perhaps the most significant difference is the increase in the multiplicity of the solutions as k decreases. For example, for the thick sphere 7 different symmetric solutions were determined at P = .07. For the thin sphere 46 different symmetric solutions were determined at P = .007.

bifurcates down from the lowest eigenvalue P_{17}. The solution branches bifurcate up from the next two unsymmetric eigenvalues P_{15} and P_{19} and have negative energy for P near the eigenvalues. We have not completely investigated the unsymmetric branches of the solution for the thin spheres. However, numerical results that are not shown in the graphs indicate that the unsymmetric solutions connect with the symmetric ones in the same way as for the thick sphere. The formation of boundary layers as P varies on $B_{16,j}$ is more pronounced for the thin sphere than for the corresponding branch of the thick sphere.

A feature of the thin sphere that has not been observed for the thick sphere is the existence of isolated solution branches. They are branches that are not connected to any of the solutions which bifurcate from the eigenvalues. For example, one of these occurs for P in the interval $.006005 < P < .010338$. There are critical loads at $P = .007760, .006095, .010338$ and $.006005$. The energies on this branch are in the interval $+.119 < (e/2)^{1/3} < .232$. Since the energy is large and positive this branch is not shown in Figure 9. We have not found any isolated branches with negative energy.

We have briefly investigated the solutions for the sphere with $k = 1.2 \times 10^{-5}$ in the neighborhood of the first few eigenvalues. The results are sketched in Figure 11. The lowest eigenvalue is symmetric. The solution branch which bifurcates from this eigenvalue has the same qualitative behavior as the

bifurcation branch from the lowest symmetric eigenvalue for $k = 10^{-3}$ and $k = 10^{-5}$. The second eigenvalue is unsymmetric and the solutions bifurcate up and have negative energy near the eigenvalue. The solutions branch down from the third eigenvalue $P = P_{15}$. They are qualitatively similar to the bifurcation branch from the lowest eigenvalue for $k = 10^{-3}$ and $k = 10^{-5}$.

5.3 Boundary Layers.

We have observed in Section 5.1, see Figures 3 and 4, that for the bifurcation branch from the lowest symmetric eigenvalue, a boundary layer forms at $\theta = \pi/2$. A second boundary layer was observed to develop at $\theta = 0$ as $k \to 0$; the solution is small everywhere except at $\theta = 0$. In Figures 12 and 13 we show the formation of this boundary layer by presenting graphs of solutions for a sequence of decreasing values of k; cf. with Figures 3 and 4. These results partially substantiate Friedrichs' conjectures [4] about the formation of "dimples" as $k \to 0$.

6. Remarks about Buckling.

We shall discuss the relevance of the results previously described to the axisymmetric buckling of perfect spherical shells under idealized experimental conditions; that is "gedanken buckling." We discuss primarily the thick sphere since our results are most comprehensive in this case. But our remarks are

equally applicable to the thin sphere and no doubt to a wide range of k values. Our basic premise is that we have determined all of the relevant axially symmetric equilibrium states of the shell for all loads in some large range: $0 \leq P \leq P_{max}$. Constant reference to Figures 1a and 2 and Table II is required for this discussion.

We imagine the pressure increasing continuously from P = 0 and allow only axisymmetric deformations. The sphere contracts radially (corresponding to the trivial solution $w \equiv 0$) for small P since this is the only existing equilibrium state. However, as soon as P exceeds $P^L_{6,1} = P^L_{6,0} \doteq .01045$, two additional equilibrium states exist corresponding to the branches $B_{6,1}$ and $B_{6,0}$. Suppose for the present that the shell does not jump or is somehow constrained from jumping to another equilibrium state. Then as the load continues to increase the sphere uniformly contracts, regardless of the numerous states which become possible, until P finally reaches the lowest eigenvalue. In the thick sphere case this is P_5. At this pressure it may be possible for the sphere to deviate from perfect sphericity without jumping by merely deforming continuously into the bifurcated mode of solution. In general if the bifurcation branch branches up (down) this smooth transition can occur only for P increasing (decreasing). Thus since $B_{5,1}$ branches down from P_5 such a smooth transition cannot occur at P_5 as P increases.*

*For other values of k, e.g. $k = 1.2\times10^{-5}$ the lowest eigenvalue is symmetric; see Figure 13. Therefore, a smooth transition into the bifurcation branch as P increases is possible.

We recall that for the bifurcation branches $B_{2m,1}$ passing through each symmetric eigenvalue P_{2m}, the energy $e_{2m,1}(P)$ is monotone decreasing. Thus as P increases beyond some P_{2m} the unbuckled state has more energy than the state on $B_{2m,1}$. If we make the reasonable assumption that at a bifurcation point states with least energy are preferred then the thick sphere smoothly deforms into the state on $B_{6,1}$ as P goes from P_5 past P_6. However, suppose the shell remains spherical as P increases beyond P_6 and P_4. Then at the unsymmetric eigenvalue P_7, whose branches $B^{\pm}_{7,1}$ bifurcate up, the smooth transition can occur onto one of the unsymmetric branches. Thus in summary, if jump-buckling is somehow prevented or just does not occur, the uniformly contracted sphere smoothly deforms into a nonspherical shape as P increases past a symmetric eigenvalue or an unsymmetric eigenvalue which branches up. We call smooth transitions to nonspherical states, as P increases, "bifurcation buckling." Then all the symmetric eigenvalues, P_{2m}, are bifurcation buckling loads and so are those unsymmetric eigenvalues, P_{2m+1}, with upward branching solutions.

Let us now consider that bifurcation buckling has occurred at $P = P_n$ and P continues to increase. The states of deformation correspond to solutions on some upward bifurcating branch $B_{n,1}$. However, as P increases beyond the upper critical point $P^U_{n,1}$ the deformation cannot vary continuously with P since the branch $B_{n,1}$ ceases to exist. Thus the shell must jump to some other non-adjacent equilibrium state. We therefore

call $P^U_{n,1}$ a jump-buckling load. Clearly, $P^U_{2m,1}$ are all jump-buckling loads and so are those $P^U_{2m+1,1}$ which are endpoints of upward bifurcating branches. For example, $P^U_{7,1} \doteq 0.0858$ for the thick sphere is a jump-buckling load while $P^U_{5,1} = P_5 = 0.0675$ is not.

Let us return to the unconstrained thick sphere experiments in which bifurcation buckling need not precede jump-buckling. As has been observed, only uniform contraction can occur for $P < P^L_{6,1}$ which we therefore term the lower buckling load P^L. Since P_5 is not a bifurcation buckling load we conclude that as P increases over the interval $P^L \doteq 0.01045 < P < P_6 \doteq 0.07062$ the thick sphere can become nonspherical only by jumping into a buckled state. The multiplicity of solutions varies over this interval. For example, at $P = 0.015$ there are eight such solutions corresponding to the branches*: $B_{6,0}$; $B_{6,1}$; $B^{\pm}_{5,1}$; $B^{\pm}_{5,2}$; $B^{\pm}_{5,7}$. Of these solutions only those on $B_{6,1}$ and $B^{\pm}_{5,1}$ have more energy than the unbuckled state at $P = 0.015$. The states with negative energy are in some sense preferred to the unbuckled state. Jumping to a state of negative energy cannot occur for $P < P^E_{6,0}$. We must invoke some mechanism for the shell to jump into one of these states of negative energy. The usual such mechanism is attributed to

*As another example consider $P = 0.01996$ where there are 16 solutions on the branches: $B_{6,0}$; $B_{6,1}$; $B^{\pm}_{5,j}$; $j = 1,2,\ldots,7$. All but the three solutions on $B_{6,1}$ and $B^{\pm}_{5,1}$ have less energy than the uniformly contracted sphere with $P = 0.01996$. In Figures 14 a,b we show 4 of these solutions.

imperfections and/or disturbances of the original spherical shell, of the loading procedure, of the shell support, etc. The transition is actually dynamic and since there are many buckled states present with energy less than the unbuckled state we do not know which state is the one finally preferred. The number and character of the buckled states which coexist at a given pressure may influence the possibility of jump-buckling. Thus the triggering mechanism which causes the shell to jump, no doubt, depends on the interaction of the imperfections, disturbances and the kind of buckled states that exist at a given pressure.

The possible buckling mechanism just described is such that precise jump-buckling loads cannot be defined. However, we note that for P just below a symmetric eigenvalue or an unsymmetric eigenvalue whose bifurcated solutions branch down there must always be buckled states very close to the unbuckled state but with slightly more energy. An example is P_5 for the thick sphere. These states could also supply the triggering mechanism for jump buckling in experiments with very small imperfections or disturbances. In such a case the observed jump buckling load should be less than the lowest eigenvalue, that is, P_5 for the thick sphere. Of course, if the imperfections are so small that they do not cause jump buckling, then as P increases bifurcation buckling must occur at P_n and finally jump buckling must occur at $P^U_{n,1}$.

We have only considered axisymmetric deformations in

this study. If we allow axially unsymmetric states there may be additional bifurcation branches and other buckled states. A numerical study of these additional bifurcation branches has not yet been initiated. However an analysis of the axially unsymmetric bifurcation branches near the eigenvalues and the effects of imperfections is given in [8] using a different shell theory.

References

1. S. Timoshenko, Theory of Elastic Stability, McGraw-Hill, New York, 1936.
2. T. von Kármán and H. S. Tsien, The Buckling of Spherical Shells by External Pressure, J. Aero. Sci. 7 (1939), pp. 43-50.
3. H. S. Tsien, A Theory for the Buckling of Thin Shells, J. Aero. Sci. 9 (1942), pp. 373-384.
4. K. O. Friedrichs, On the Minimum Buckling Load for Spherical Shells, von Kármán Anniversary Volume, Calif. Inst. Tech., Pasadena, 1941, pp. 258-272.
5. B. Altshuler, Nonlinear Buckling of a Spherical Shell, Doctoral thesis, New York Univ., 1953.
6. A. G. Gabril'iants and V. I. Feodos'ev, Axially-Symmetric Forms of Equilibrium of an Elastic Spherical Shell under Uniformly Distributed Pressure, PMM, 25 (1961), pp. 1091-1101. (Engl. transl. in J. Appl. Math. Mech. 25 (1961), pp. 1629-1642.)
7. T. Koga and N. J. Hoff, The Axisymmetric Buckling of Initially Imperfect Complete Spherical Shells, Int. J. Solids and Structures 5 (1969), pp. 679-697.
8. W. T. Koiter, The Nonlinear Buckling Problem of a Complete Spherical Shell under Uniform External Pressure, Rep. No. 412, Lab. of Eng. Mech., Technological Univ., Delft, 1968.

9. J. M. T. Thompson, The Rotationally Symmetric Branching Behaviour of a Complete Spherical Shell, Proc. Koninkl. Nederl. Akad. van Wet. Amsterdam, Sec. B, 6 (1964), pp. 295-311.

10. E. L. Reiss, H. J. Greenberg and H. B. Keller, Nonlinear Deflections of Shallow Spherical Shells, J. Aero. Sci. 24 (1957), pp. 533-543.

11. S. Timoshenko, Theory of Plates and Shells, McGraw-Hill, New York, 1940.

12. E. Bromberg and J. J. Stoker, Nonlinear Theory of Curved Elastic Sheets, Q. Appl. Math. 3 (1945), pp. 246-265.

13. T. M. MacRobert, Spherical Harmonics, Dover, New York, 1948.

14. H. B. Keller, Numerical Methods for Two Point Boundary Value Problems, Ginn-Blaisdell, Waltham, Mass., 1968.

15. W. Langford, Bifurcation Theory of Thin Spheres, in preparation.

Appendix I. Derivation of the Shell Theory.

The two dimensional Hooke's law for the normal stresses σ_θ and σ_ϕ is

$$(A.1) \qquad \sigma_\theta = \frac{E}{1-\nu^2}(E_\theta + \nu E_\phi) , \quad \sigma_\phi = \frac{E}{1-\nu^2}(E_\phi + \nu E_\theta) .$$

Substituting (2.7) and (2.8) into (A.1) yields

$$(A.2a) \qquad \sigma_\theta(r,\theta) = ES(\theta) - z(\frac{3ER}{h^2})M , \quad \sigma_\phi(r,\theta) = ET(\theta) - z(\frac{3ER}{h^2})N ,$$

where

$$(A.2b) \quad \begin{cases} S(\theta) = (1-\nu^2)^{-1}(e_\theta+\nu e_\phi) = (1-\nu^2)^{-1}[U'-W+\frac{1}{2}V^2+\nu(U\cot\theta-W)], \\ T(\theta) = (1-\nu^2)^{-1}(e_\phi+\nu e_\theta) = (1-\nu^2)^{-1}[U\cot\theta-W+\nu(U'-W+\frac{1}{2}V^2)], \end{cases}$$

and

$$(A.2c) \quad \begin{cases} M(\theta) = \frac{Rk}{1-\nu^2}(\kappa_\theta + \nu\kappa_\phi) = \frac{k}{1-\nu^2}(V' + \nu V\cot\theta) , \\ N(\theta) = \frac{Rk}{1-\nu^2}(\kappa_\phi + \nu\kappa_\theta) = \frac{k}{1-\nu^2}(V\cot\theta + \nu V') . \end{cases}$$

The parameter k is defined in (2.9c). The dimensionless quantities S and T are proportional to σ_θ and σ_ϕ evaluated on the middle surface, z = 0. They are called the membrane stresses. The dimensionless quantities M and N, which we call the bending moments, are related to the physical bending moments M_θ and M_ϕ by

$$M = -M_\theta/(2EhR) , \qquad N = -M_\phi/(2EhR) .$$

The strain energy of the shell is given approximately by

$$(A.3) \qquad I \equiv \frac{1}{2}\int_{R-h}^{R+h}\int_{0}^{2\pi}\int_{0}^{\pi}(\sigma_\theta E_\theta + \sigma_\phi E_\phi)r^2 \sin\theta \, d\theta \, d\phi \, dr \, .$$

We insert (2.4), (2.7), (2.8), (A.1) and (A.2) into (A.3), perform the r, ϕ integrations and use $h/R << 1$ to obtain

$$(A.4) \quad I = 2\pi R^2 Eh \int_0^{\pi} [(Se_\theta + Te_\phi) + R(M\kappa_\theta + N\kappa_\phi)]\sin\theta \, d\theta \, .$$

If p is a pressure then the work done, F, is defined by

$$(A.5) \qquad F = -p\Delta$$

where Δ is the change in the volume enclosed by the midsurface of the shell before and after deformation. The pressure is positive when it is directed inwards. To determine Δ we first denote the projections on the equatorial plane and on the polar axis* of the radius from the origin to any point on the shell's mid-surface respectively by ρ and δ. Thus for the undeformed shell we have

$$(A.6) \qquad \rho = \rho_u \equiv R \sin\theta, \qquad \delta = \delta_u \equiv R\cos\theta \, ,$$

and for the deformed shell we have

$$(A.7) \qquad \rho = \rho_d \equiv R\sin\theta + H, \quad \delta = \delta_d \equiv R\cos\theta - J \, .$$

Here H and J, the horizontal and vertical components of the displacement of a point on the shell's mid-surface, are given by

*The polar axis is the diameter through the north and south poles. We assume the shell is oriented so that the polar axis is vertical. The equatorial plane, defined by $\theta = \pi/2$, $0 \leq \phi \leq 2\pi$, is thus horizontal.

(A.8) $\frac{H}{R} = (U \cot\theta - W)\sin\theta = e_\phi \sin\theta, \quad \frac{J}{R} = W\cos\theta + U\sin\theta.$

J is positive downwards. Δ is defined by

$$\Delta \equiv \pi \int_0^\pi (\rho_u^2 \delta_u' - \rho_d^2 \delta_d') \, d\theta \, . \tag{A.9}$$

We substitute (A.6)-(A.8) into (A.9) and use (2.8a) to get

$$\Delta = \pi R^3 \int_0^\pi [e_\phi^3 + 3e_\phi + 3e_\phi^2) + (U' + W' \cot\theta)(1 \pm e_\phi)^2] \sin^3\theta \, d\theta. \tag{A.10}$$

Since $|e_\phi| << 1$, Δ is given approximately by

$$\Delta = \pi R^3 \int_0^\pi [U' + W' \cot\theta + 3e_\phi] \sin^3\theta \, d\theta \, . \tag{A.11}$$

Employing the expression for e_ϕ given by (2.8a) in (A.11), we obtain after integration by parts,

$$\Delta = -2\pi R^3 \int_0^\pi W \sin\theta \, d\theta \quad . \tag{A.12}$$

Thus from (A.5) and (A.12) the work done by the normal pressure is

$$F = 2\pi R^3 p \int_0^\pi W \sin\theta \, d\theta \quad . \tag{A.13}$$

We observe that (A.13) is also the work done by a uniformly distributed surface force p which is directed toward r = 0. Hence, <u>for this shell theory, normal pressure and a centrally directed surface load have, within terms of higher order, the same work expression</u>. Consequently the boundary value problems will be the same for both loads.

The potential energy G is defined as

(A.14) $$G \equiv I - F ,$$

where I and F are given by (A.4) and (A.13). Employing (2.6), (2.8) and (A.2b,c) in (A.14), we express G as a functional of u and w. The Euler equations of this functional are

(A.15a) $$Q \sin\theta + (S \sin\theta)' - T \cos\theta = 0 ,$$

(A.15b) $$(Q \sin\theta)' - (S+T)\sin\theta - 2P \sin\theta = 0 ,$$

where the shear Q is defined by

(A.15c) $$Q = [(M \sin\theta)' - N \cos\theta - SV \sin\theta]\csc\theta ,$$

and P is defined in (2.9c). Since the solutions are to be bounded and axisymmetric with respect to the polar axis the boundary conditions at $\theta = 0,\pi$ are

(A.16) $$U = W' = Q = 0 .$$

We observe that

(A.17) $$U = V = M = N = Q = 0, \quad S = T = -P, \quad W = W_0 \equiv (1-\nu)P ,$$

is a solution, for all P and k, of the system of equations (A.2), (A.15), (2.6) and satisfies the boundary conditions (A.16). It represents the uniformly contracted sphere or the unbuckled state. We seek other solutions in the form

$$W = W_0 + w(\theta) , \quad S = -P + s(\theta) , \quad T = -P + t(\theta) ,$$

(A.18)

$$U = u(\theta) , \quad V = v(\theta) , \ldots, Q = q(\theta) .$$

We substitute (A.18) into (A.2), (A.15), (2.6) and (A.16) and find that the lower case variables must satisfy

(A.19a) $$q \sin\theta + (s \sin\theta)' - t \cos\theta = 0 ,$$

(A.19b) $$(q \sin\theta)' - (s+t)\sin\theta = 0 ,$$

(A.19c) $$(m \sin\theta)' - n \cos\theta - sv \sin\theta - q \sin\theta + Pv \sin\theta = 0,$$

(A.19d) $$v = u + w' ,$$

(A.19e)
$$\begin{cases} s = \left(\frac{1}{1-\nu^2}\right)[u' - w + \frac{1}{2} v^2 + \nu(u \cot\theta - w)] , \\ t = \left(\frac{1}{1-\nu^2}\right)[u \cot\theta - w + \nu(u' - w + \frac{1}{2} v^2)] , \end{cases}$$

(A.19f)
$$\begin{cases} m = \frac{1}{1-\nu^2} (v' + \nu v \cot\theta) , \\ n = \frac{1}{1-\nu^2} (v \cot\theta + \nu v') , \end{cases}$$

(A.19g) $$u = w' = q = 0 , \quad \theta = 0, \pi .$$

Equations (A.19a-f) are a system of eight equations in eight dependent variables. We eliminate the four variables s, n, u and w from this system and obtain the four ordinary differential equations (2.9a,b). The boundary conditions (2.14) follow from (A.19d,g). When a solution of this boundary value problem is determined we evaluate the eliminated variables from

(A.20) $$s = q \cot\theta , \quad n = \nu m + kv \cot\theta .$$

The equations to evaluate u and w are obtained by first eliminating w from (A.19e). This yields the first order ordinary differential equation for u, (2.18).

If G_0 is the potential energy of the unbuckled state (A.17), then the relative potential energy e of a buckled state is

(A.21) $$e \equiv G - G_0 \ .$$

We insert (A.4) and (A.13) in (A.14) and express G in terms of m, q, t, v and w. Integration by parts and (A.19g) gives (2.19).

Figure 1a

Graphs of P vs. the amplitude A, which is defined in Equation (5.1), corresponding to the 7 lowest symmetric eigenvalues and the 4 lowest unsymmetric eigenvalues for the thick sphere $k = .001$. The circles on the P axis indicate the symmetric eigenvalues and the crosses the unsymmetric eigenvalues. Several of the lower symmetric branches $B_{n,j}$ and the lower unsymmetric branches $B^{\pm}_{n,j}$ are explicitly labeled in the graph. Several of the upper $P^{U}_{n,j}$ and lower $P^{L}_{n,j}$ critical loads are also shown. The branches $B^{\pm}_{5,j}$, $j = 1,2,\ldots,7$ and $B_{6,1}$ and $B_{6,0}$ are not completely shown in the figure since the corresponding values of A are too large. They are shown in Figure 1b. The circles on the graphs indicate the pressures at which unsymmetric branches merge with symmetric branches.

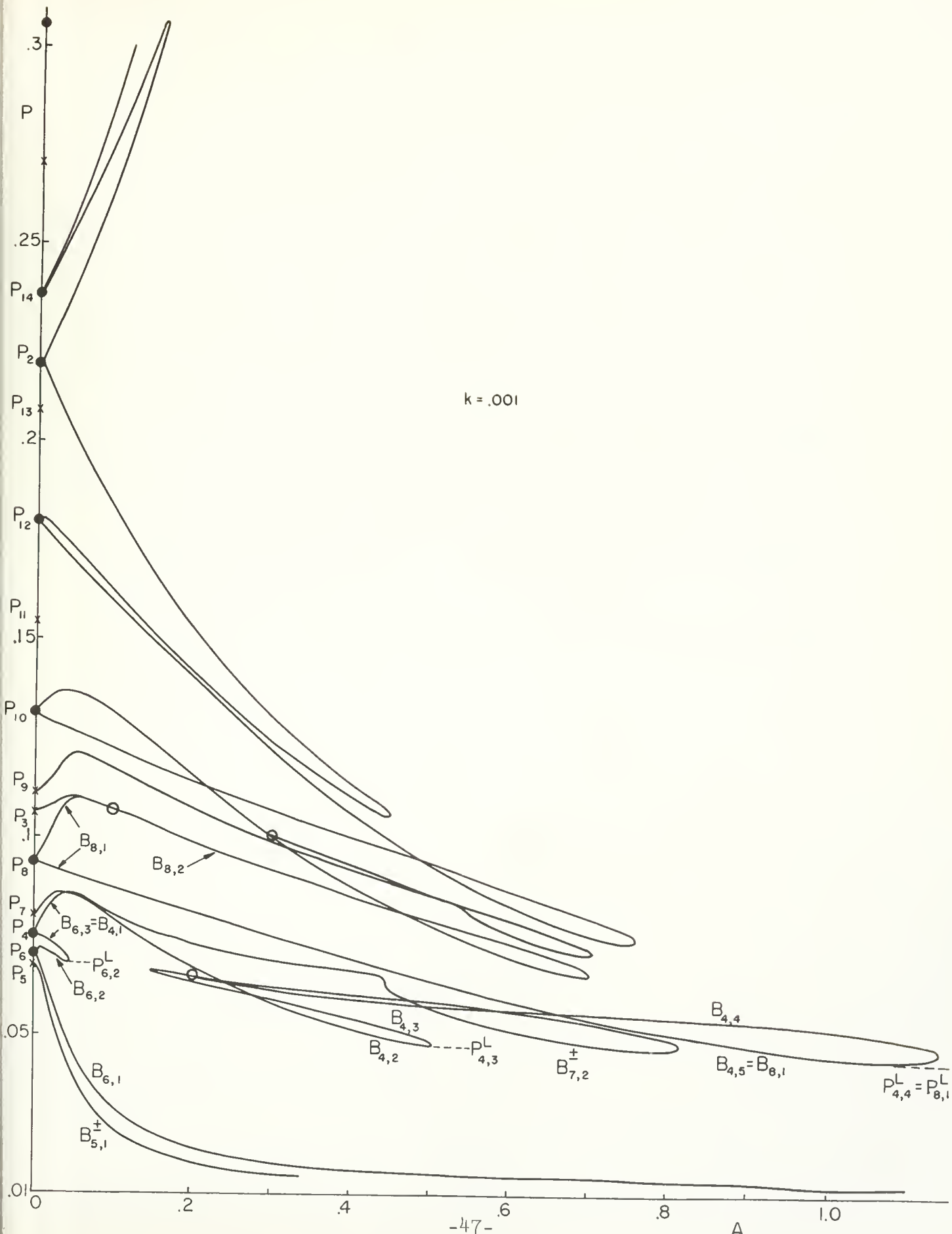
.3
P
.25
P14
P2
P13
.2
P12
P11
.15
P10
P9
P3
.1
P8
P7
P4
P6
P5
.05
.01
k = .001
B8,1
B8,2
B6,3=B4,1
P6,2
B6,2
B6,1
B5,1
B4,3
B4,2
P4,3
B7,2
B4,4
B4,5=B8,1
P4,4=P8,1
0
.2
.4
.6
.8
1.0
A

Figure 1b

Graphs of P vs. A for $B_{6,1}$ with $P \leq P_6$, $B_{6,0}$ and $B^{\pm}_{5,j}$, $j = 1,2,\ldots,7$. The scale of the graph is insufficient to resolve the branches $B^{\pm}_{5,j}$, $j = 2,\ldots,7$ completely. The unsymmetric branches $B^{\pm}_{5,7}$ merge with the symmetric branch $B_{6,1}$ at $P = P^{L}_{5,7} \doteq 0.0124$. The circle on the graph indicates the pressure at which $B^{\pm}_{5,7}$ merge with $B_{6,1}$.

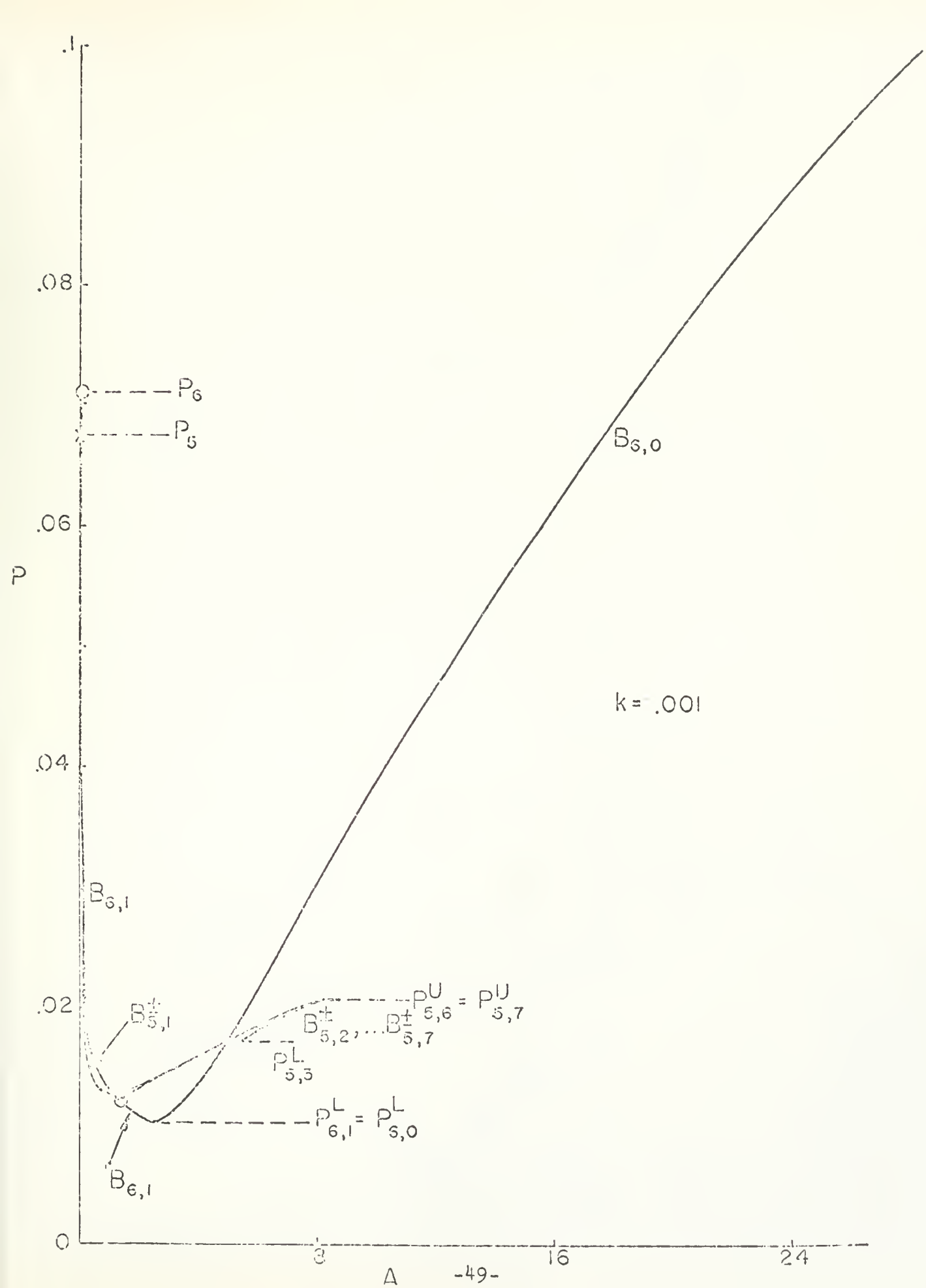
.1
.08
.06
.04
.02
0
P
A
3
16
24
P_6
P_5
$B_{6,0}$
k = .001
$B_{6,1}$
$B^{\pm}_{5,1}$
$P^{U}_{5,6} = P^{U}_{5,7}$
$B^{\pm}_{5,2}, \ldots B^{\pm}_{5,7}$
$P^{L}_{5,3}$
$P^{L}_{6,1} = P^{L}_{5,0}$
$B_{6,1}$

Figure 2a

Graphs of $(e/2)^{1/3}$ vs. P for the thick sphere, k = .001. The P axis is horizontal. The circles on the P axis indicate the symmetric eigenvalues and the crosses the unsymmetric eigenvalues. Some of the critical loads and branches are labeled. The circles on the graphs indicate the pressures at which unsymmetric branches merge with symmetric branches. The equal energy loads $P^E_{n,j}$ occur where the curves cross the P axis at points other than eigenvalues. The $P^E_{n,j}$ are too close to P_n to be clearly shown on $B_{n,j}$ with $n \geq 12$. The branches $B_{6,0}$ and $B_{5,j}$, $j = 2,3,\ldots,7$ are not completely shown in this figure since the values of $-(e/2)^{1/3}$ are too large. They are shown in Figure 2b.

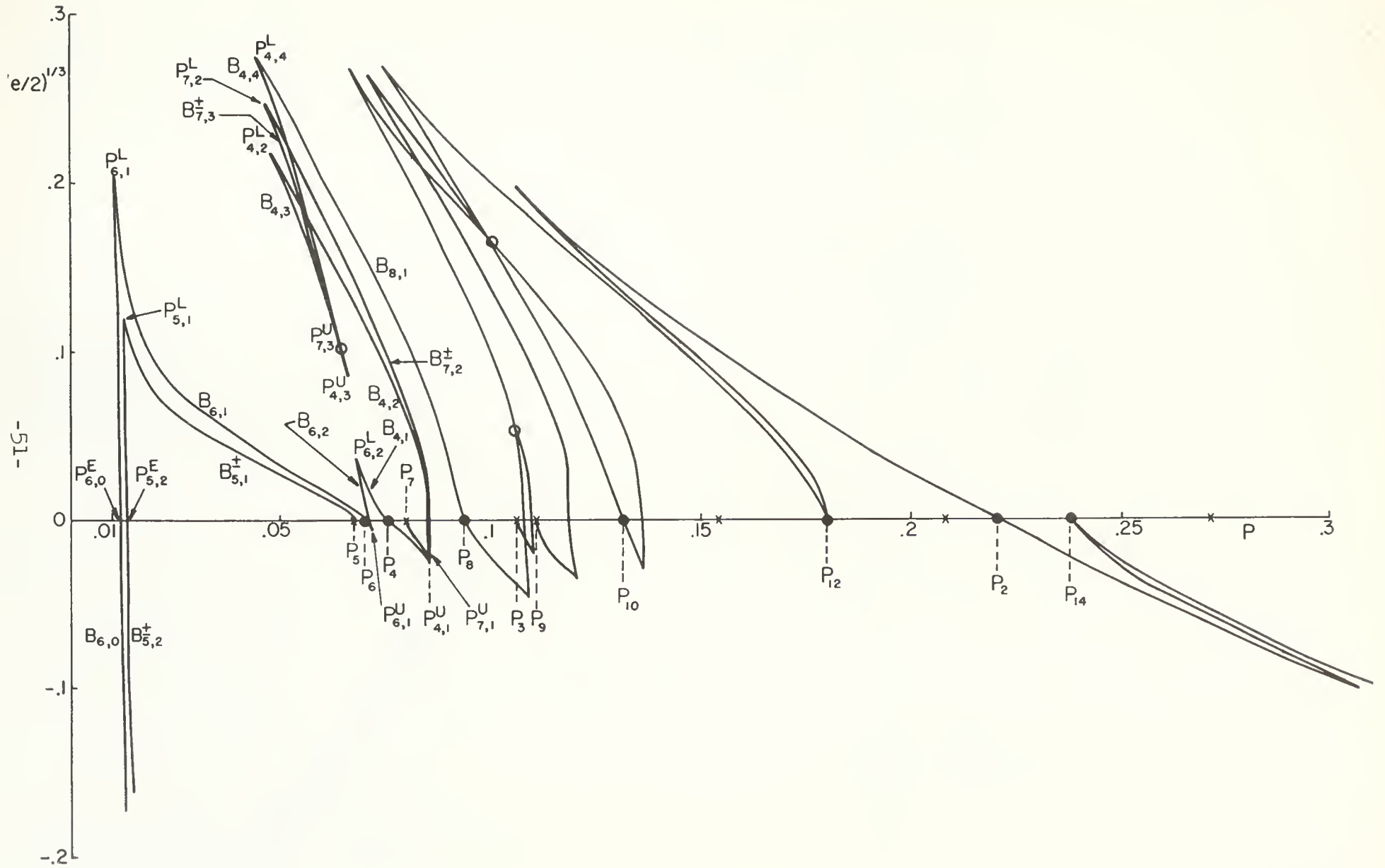
.3
.2
.1
0
-.1
-.2
(e/2)^1/3
P
.01
.05
.1
.15
.2
.25
.3
$P^L_{4,4}$
$P^L_{7,2}$
$B_{4,4}$
$B^{\pm}_{7,3}$
$P^L_{4,2}$
$B_{4,3}$
$P^L_{6,1}$
$B_{8,1}$
$P^L_{5,1}$
$P^U_{7,3}$
$B^{\pm}_{7,2}$
$P^U_{4,3}$
$B_{4,2}$
$B_{6,1}$
$B_{6,2}$
$B_{4,1}$
$P^L_{6,2}$
$P^E_{6,0}$
$P^E_{5,2}$
$B^{\pm}_{5,1}$
P_7
P_5
P_6
P_4
P_8
$P^U_{6,1}$
$P^U_{4,1}$
$P^U_{7,1}$
P_3
P_9
P_{10}
P_{12}
P_2
P_{14}
$B_{6,0}$
$B^{\pm}_{5,2}$

Figure 2b

Graphs of $(e/2)^{1/3}$ vs. P for the lower part of the branches bifurcating from the lowest two eigenvalues P_5 and P_6. The eigenvalues are not shown on the graph since their magnitudes exceed the scale. The branch $B_{6,0}$ has been continued as far as P = .1, where $(e/2)^{1/3} \doteq -1.4$. N(P) denote the number of buckled solutions for P in the interval $\underline{P} < P < \overline{P}$. The following table shows how N varies for the range of P given in the figure.

$\overline{P}$	$P^L_{6,1}$	$P^L_{5,7}$	$P^L_{5,1}$	$P^L_{5,3}$	$P^L_{5,5}$	$P^U_{5,4}$	$P^U_{5,2}$	$P^U_{5,6}$
$\underline{P}$	0	$P^L_{6,1}$	$P^L_{5,7}$	$P^L_{5,1}$	$P^L_{5,3}$	$P^L_{5,5}$	$P^U_{5,4}$	$P^U_{5,2}$
N	0	2	4	8	12	16	12	8

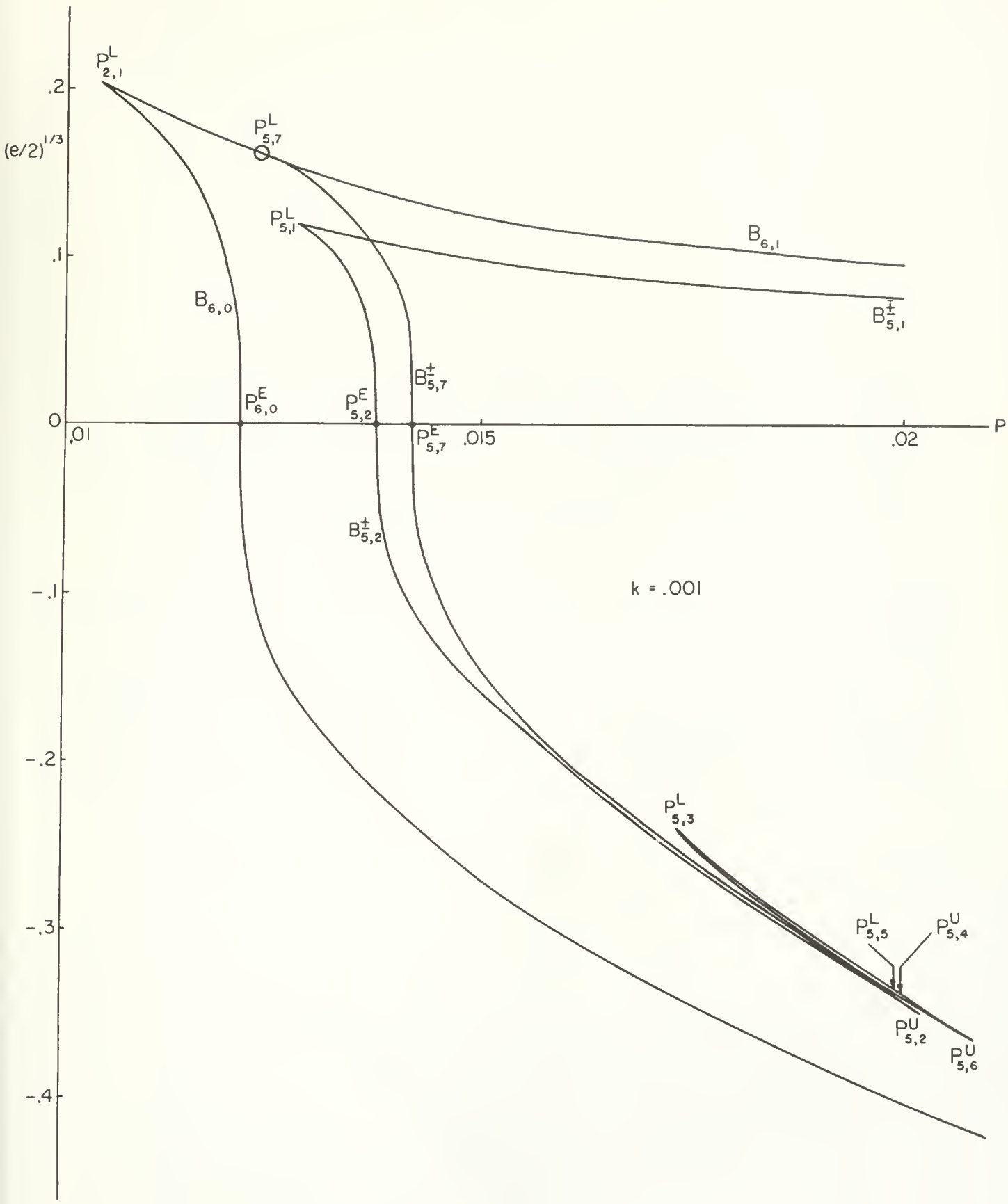
$P^L_{2,1}$
$P^L_{5,7}$
$P^L_{5,1}$
$B_{6,1}$
$B^{\pm}_{5,1}$
$B_{6,0}$
$B^{\pm}_{5,7}$
$P^E_{6,0}$
$P^E_{5,2}$
$P^E_{5,7}$
$B^{\pm}_{5,2}$
$P^L_{5,3}$
$P^L_{5,5}$
$P^U_{5,4}$
$P^U_{5,2}$
$P^U_{5,6}$
$(e/2)^{1/3}$
.2
.1
0
-.1
-.2
-.3
-.4
.01
.015
.02
P
k = .001

Figure 3

Graphs of the radial displacement $W(\theta) \equiv w(\theta) + W_0$, where W_0 is the uniform radial contraction of the unbuckled state. The solutions are for a sequence of values of P as indicated in the following table. This table also applies to Figure 4.

Graph Number	1	2	3	4	5	6	7	8	9	10	11	12	13
P	P_6	.06	.04	.03	.02	.015	.013	.011	.0105	.0105	.03	.075	.1
Branch	$B_{6,1}$	←						→	$B_{6,1}$	$B_{6,0}$	←	→	$B_{6,0}$

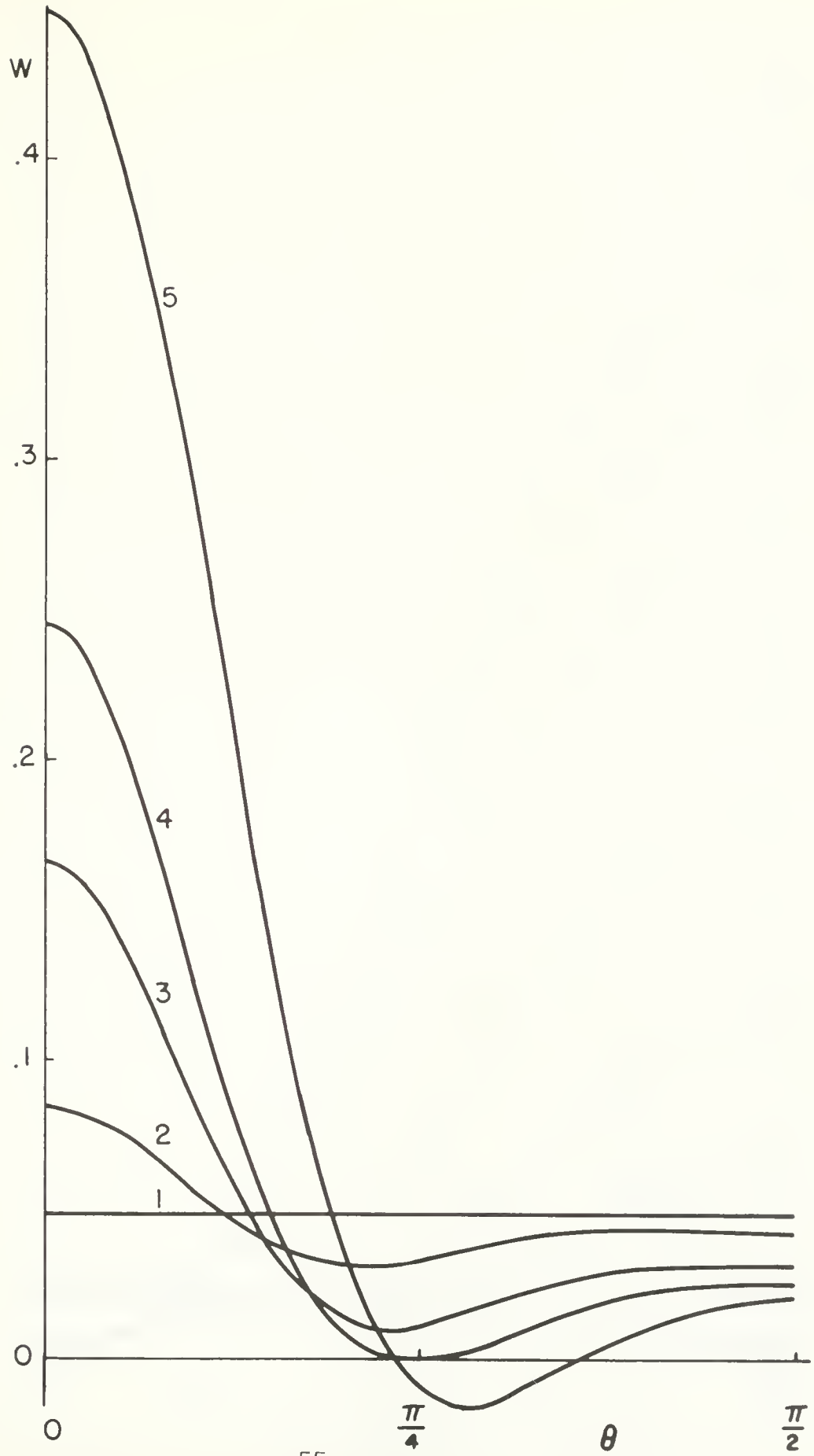
W
.4
.3
.2
.1
0
5
4
3
2
1
0
π/4
θ
π/2

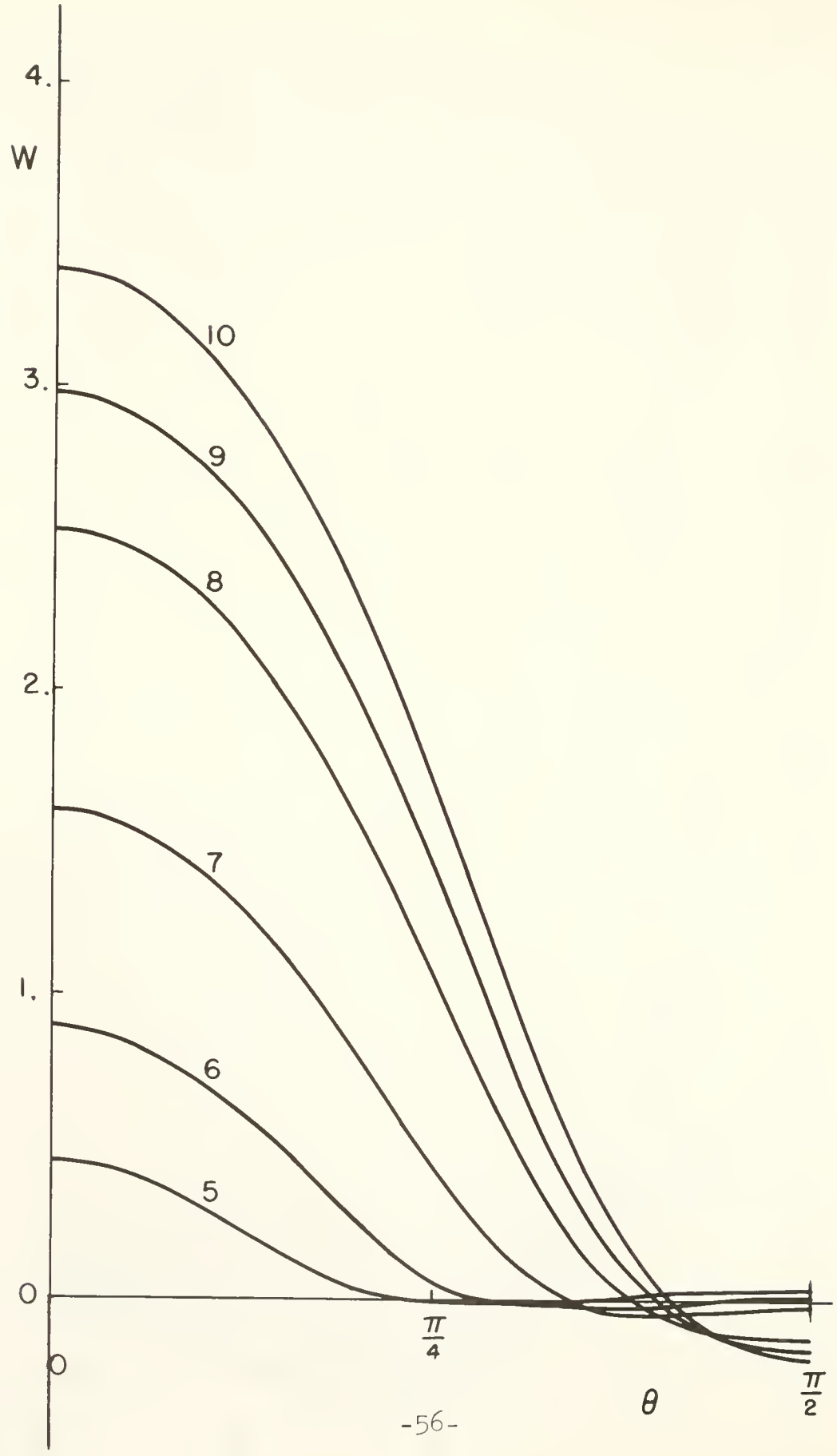
4.
W
3.
2.
1.
0
10
9
8
7
6
5
0
$\frac{\pi}{4}$
θ
$\frac{\pi}{2}$

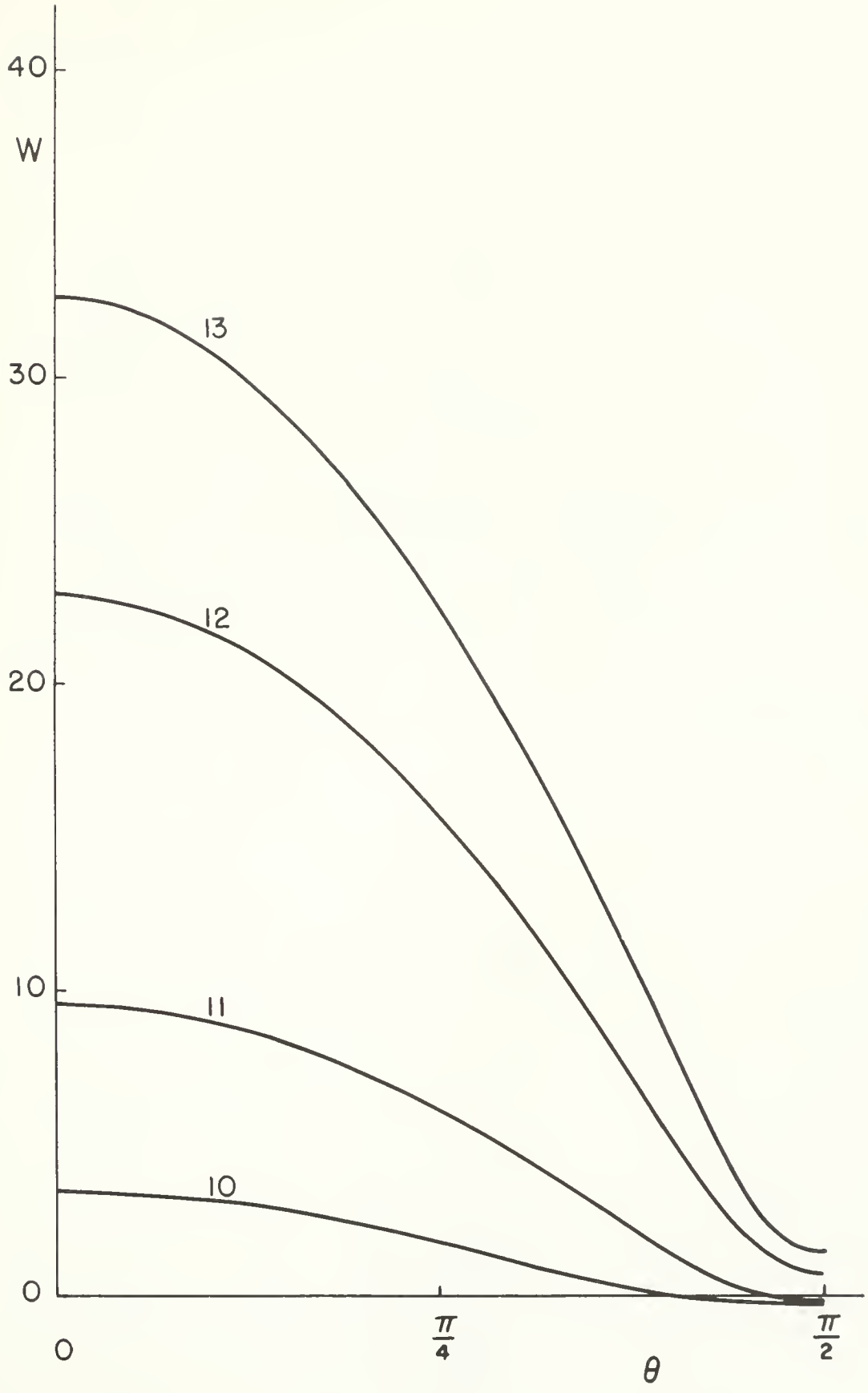
40
W
30
20
10
0
13
12
11
10
0
π/4
π/2
θ

Figure 4

Graphs of the reduced circumferential stress $t(\theta)$, see Eq. (A.18). The solutions are for the sequence of P values given in the table in the caption for Figure 3.

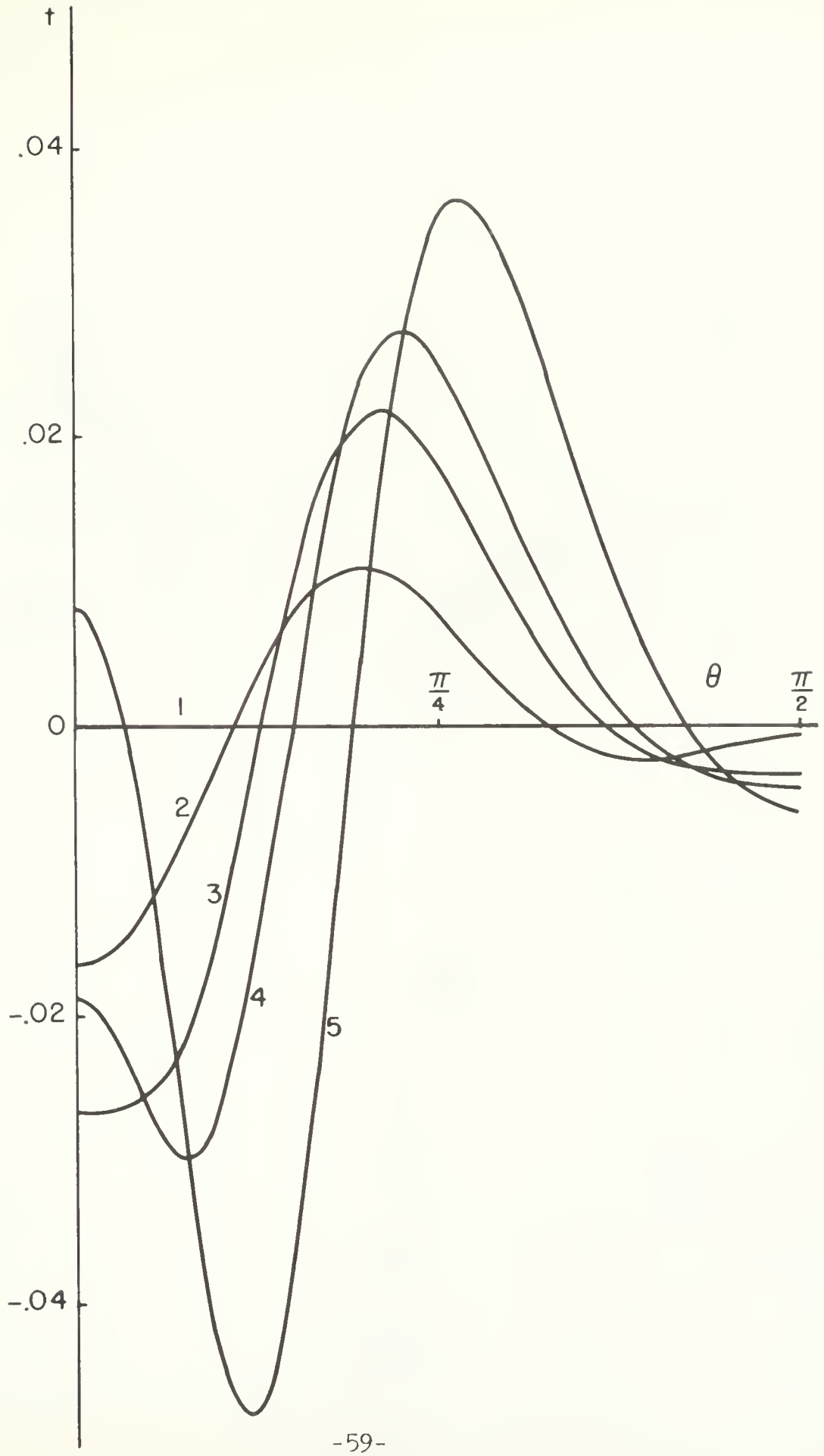
t
.04
.02
0
-.02
-.04
θ
π/4
π/2
1
2
3
4
5

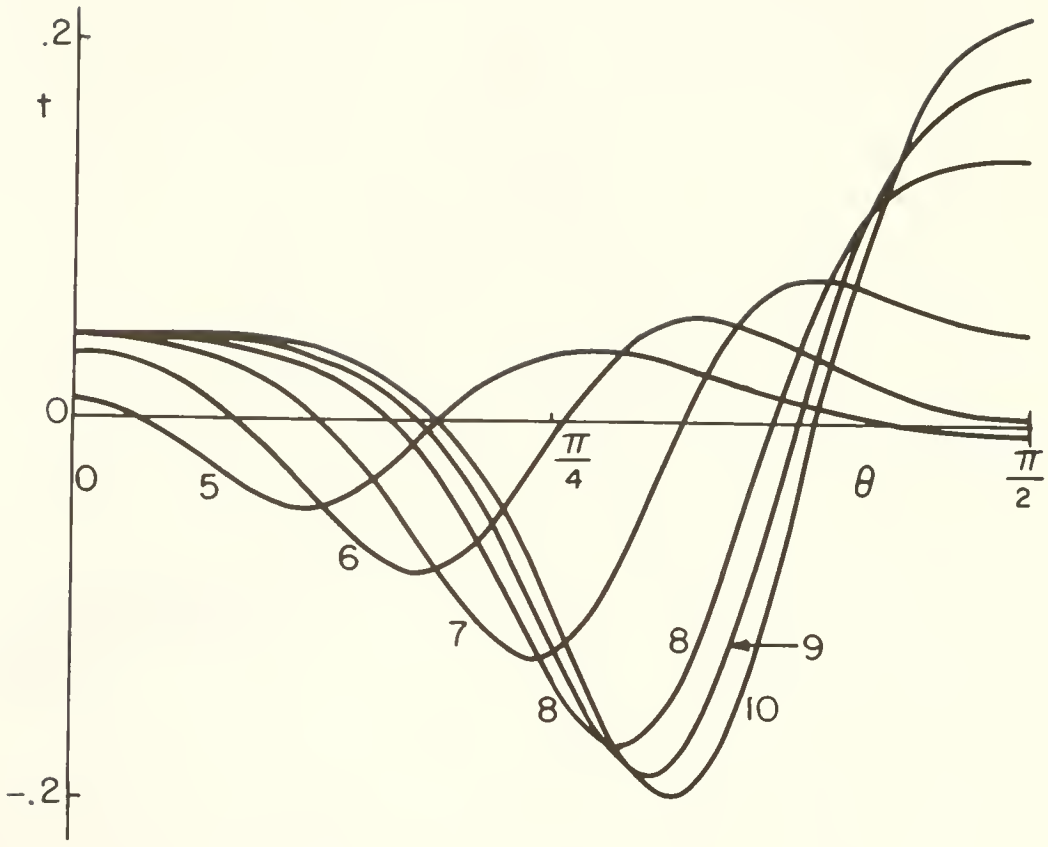
.2
t
0
-.2
0
5
6
7
8
8
9
10
π/4
θ
π/2

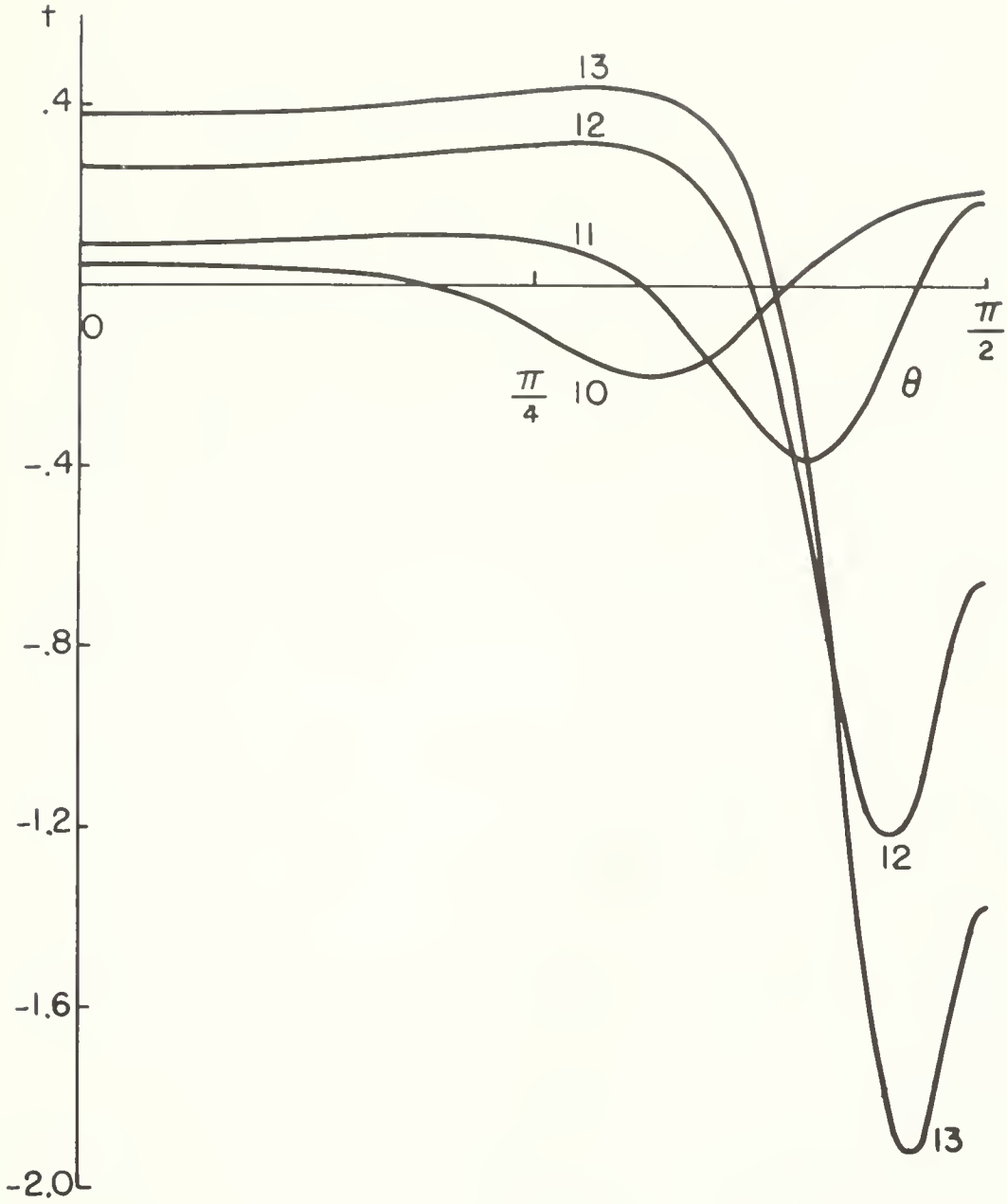
t
.4
-.4
-.8
-1.2
-1.6
-2.0
13
12
11
10
0
π/4
π/2
θ
12
13

Figure 5

Graphs of $W(\theta)$ for a sequence of values of P to show the transition in buckled shapes from $B_{6,1}$ to $B_{6,2}$ to $B_{4,1}$. The graphs numbered 1 and 4 are for P near the eigenvalues P_6 and P_4. The graphs numbered 2 and 3 are for P near the critical loads $P^U_{6,1}$ and $P^L_{6,2}$.

Graph Number	1	2	3	4
P	.070	.0712594 $\doteq P^U_{6,1} = P^U_{6,2}$	0.678672 $\doteq P^L_{6,2} = P^L_{4,1}$	.074
Branch	$B_{6,1}$	$B_{6,1}$ or $B_{6,2}$	$B_{6,2}$ or $B_{4,1}$	$B_{4,1}$

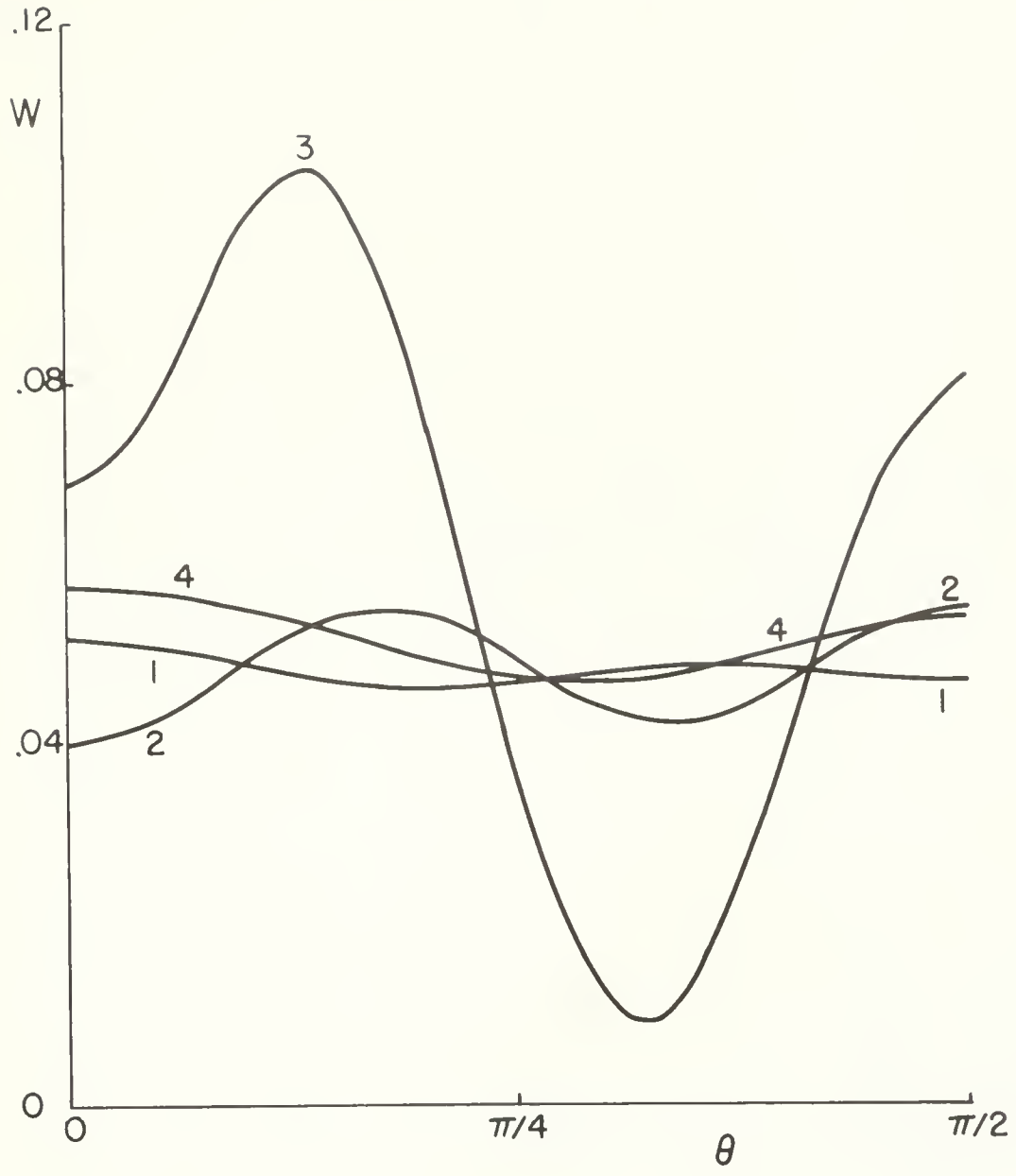
.12
W
.08
.04
0
0
π/4
π/2
θ
3
4
1
2
4
2
1

Figure 6

Graphs of $t(\theta)$ for the same sequence of values of P as given in the table of the caption for Figure 5.

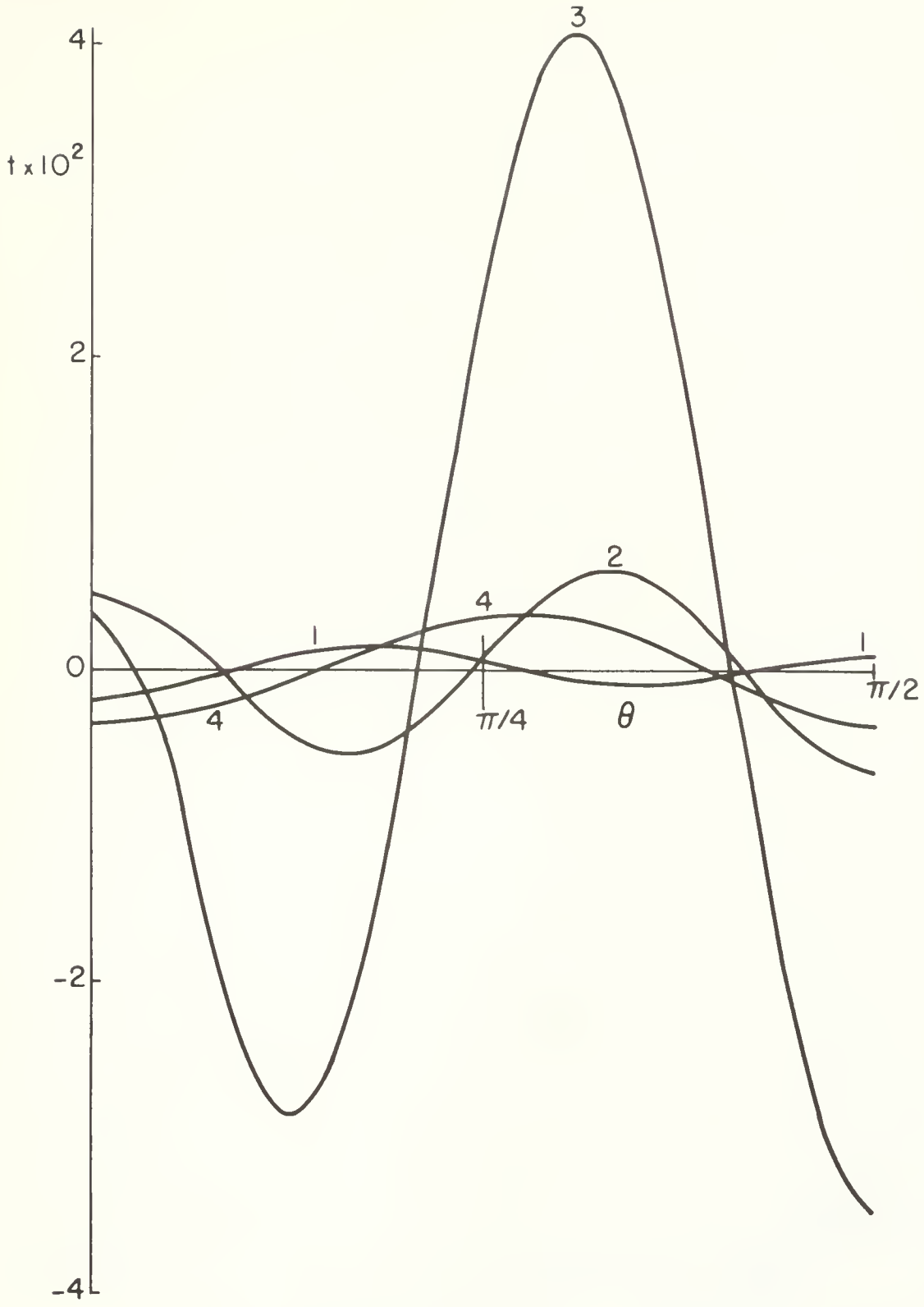
4
t x 10²
2
0
-2
-4
3
2
4
1
1
4
π/4
θ
π/2

Figure 7a

Graphs of $W(\theta)$ corresponding to points on $B^{+}_{5,1}$ for a sequence of decreasing P values. Graphs 1, 2 and 3 are respectively for P = .066, .061, .040.

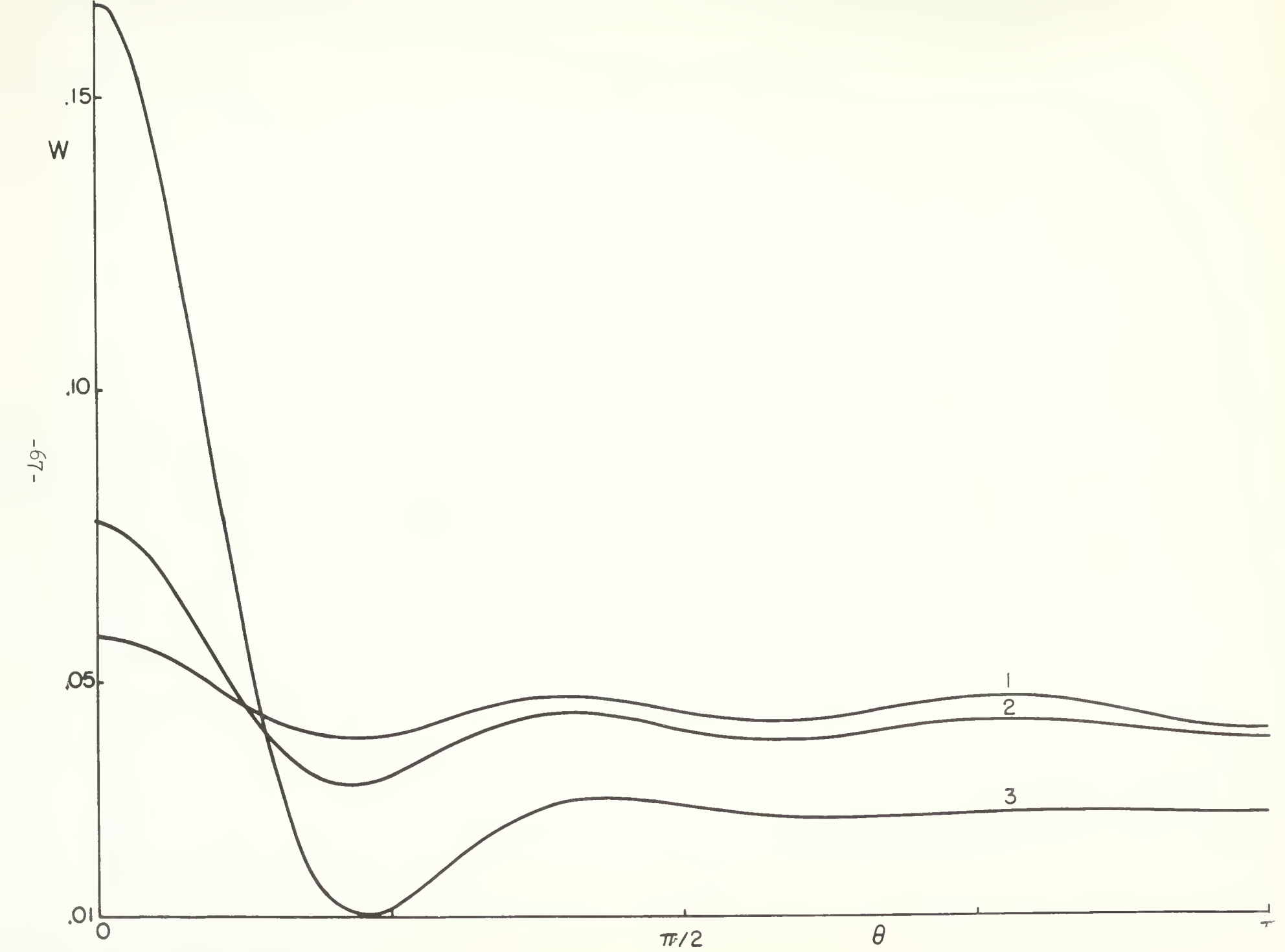
.15
W
.10
.05
.01
0
π/2
θ
1
2
3

Figure 7b

Graphs of $W(\theta)$ for a sequence of values of P on $B^{+}_{5,j}$ with j increasing. The purpose of the figure is to show how the unsymmetric solutions gradually merge with the symmetric solution at $P = P^{L}_{5,7} \doteq .012397$. Graphs 4, 5, 6 and 7 are respectively for $P = .0128125 \doteq P^{L}_{5,1} = P^{L}_{5,2}$, $P = .0173426 \doteq P^{L}_{5,3} = P^{L}_{5,4}$, $P = .020854 \doteq P^{U}_{5,6} = P^{U}_{5,7}$, and $P = .013$. The curve 7 is on $B^{+}_{5,7}$ near $P^{L}_{5,7}$ where the unsymmetric and symmetric solutions merge.

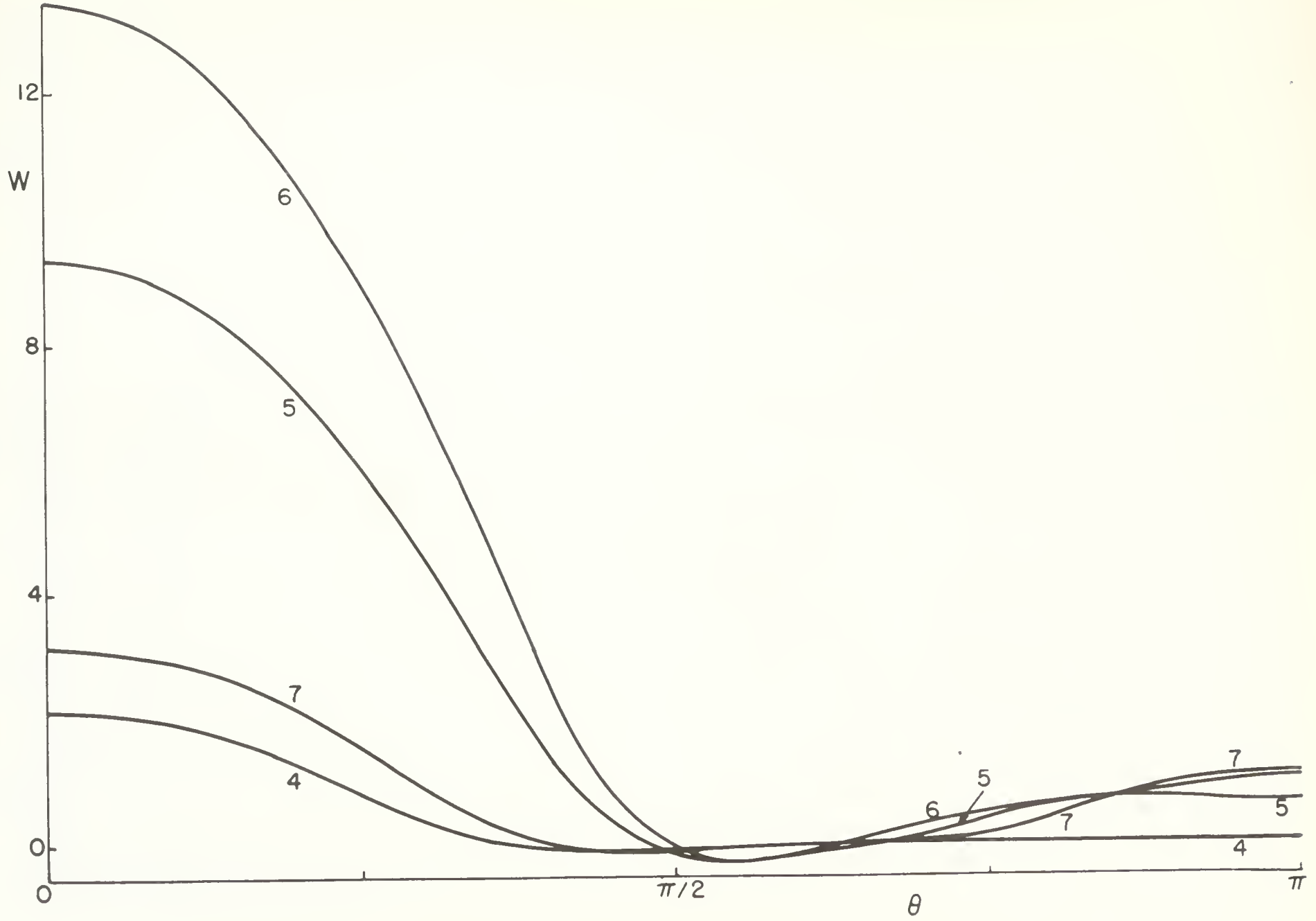
12
W
8
4
0
0
π/2
θ
π
6
5
7
4
7
5
6
7
4

Figure 8a

Graphs of $t(\theta)$ corresponding to points on $B^{+}_{5,1}$ for the same values of P as in Figure 7a.

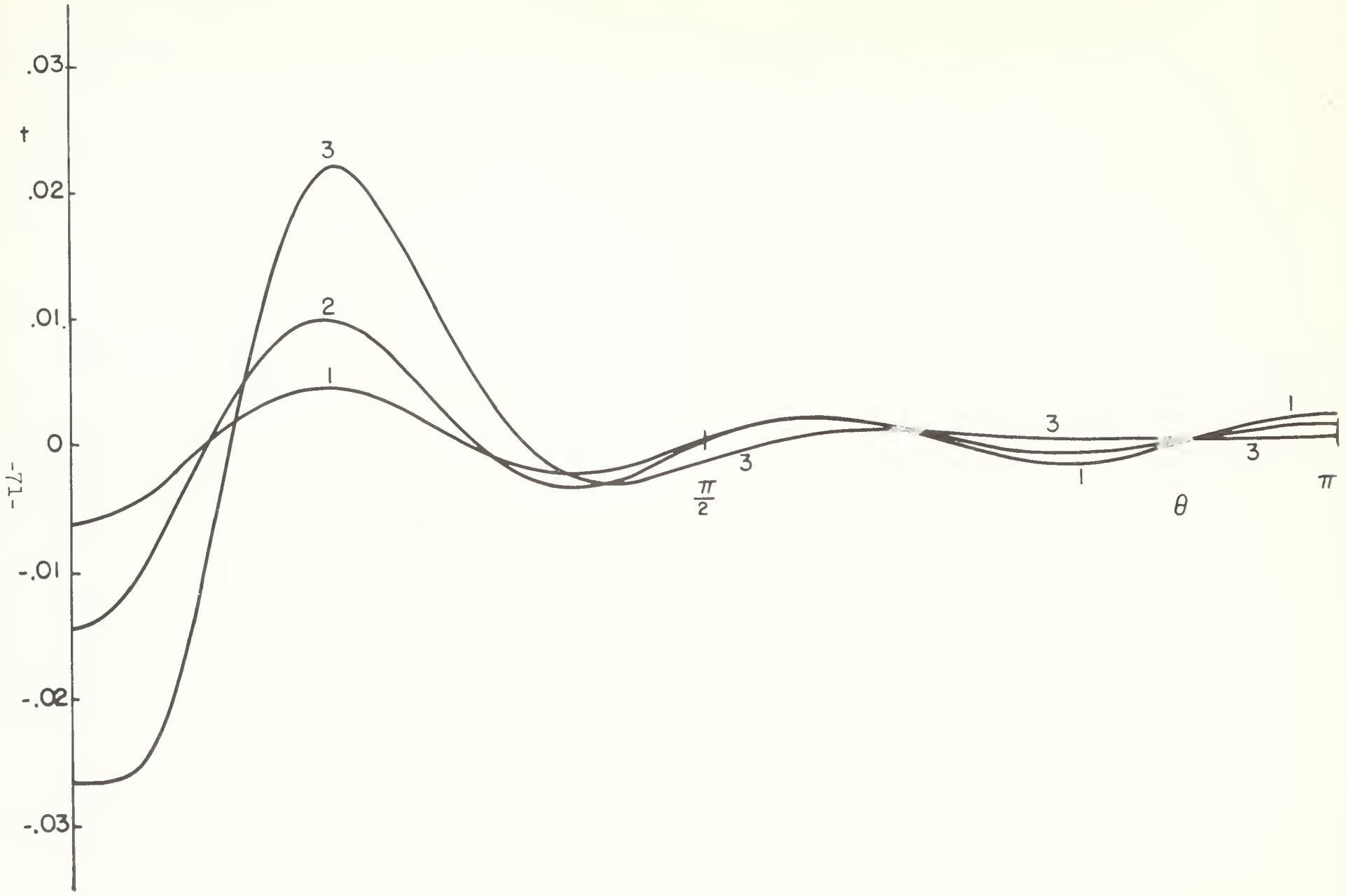
.03
t
.02
.01
0
-.01
-.02
-.03
3
2
1
3
1
3
1
3
1
$\frac{\pi}{2}$
θ
π
-71-

Figure 8b

Graphs of $t(\theta)$ corresponding to the same solutions and pressures as in Figure 7b and in addition Graph 8 for P = .012399. Since P = .012399 is close to $P^{L}_{5,7} \doteq .0123971$ this solution is nearly symmetric.

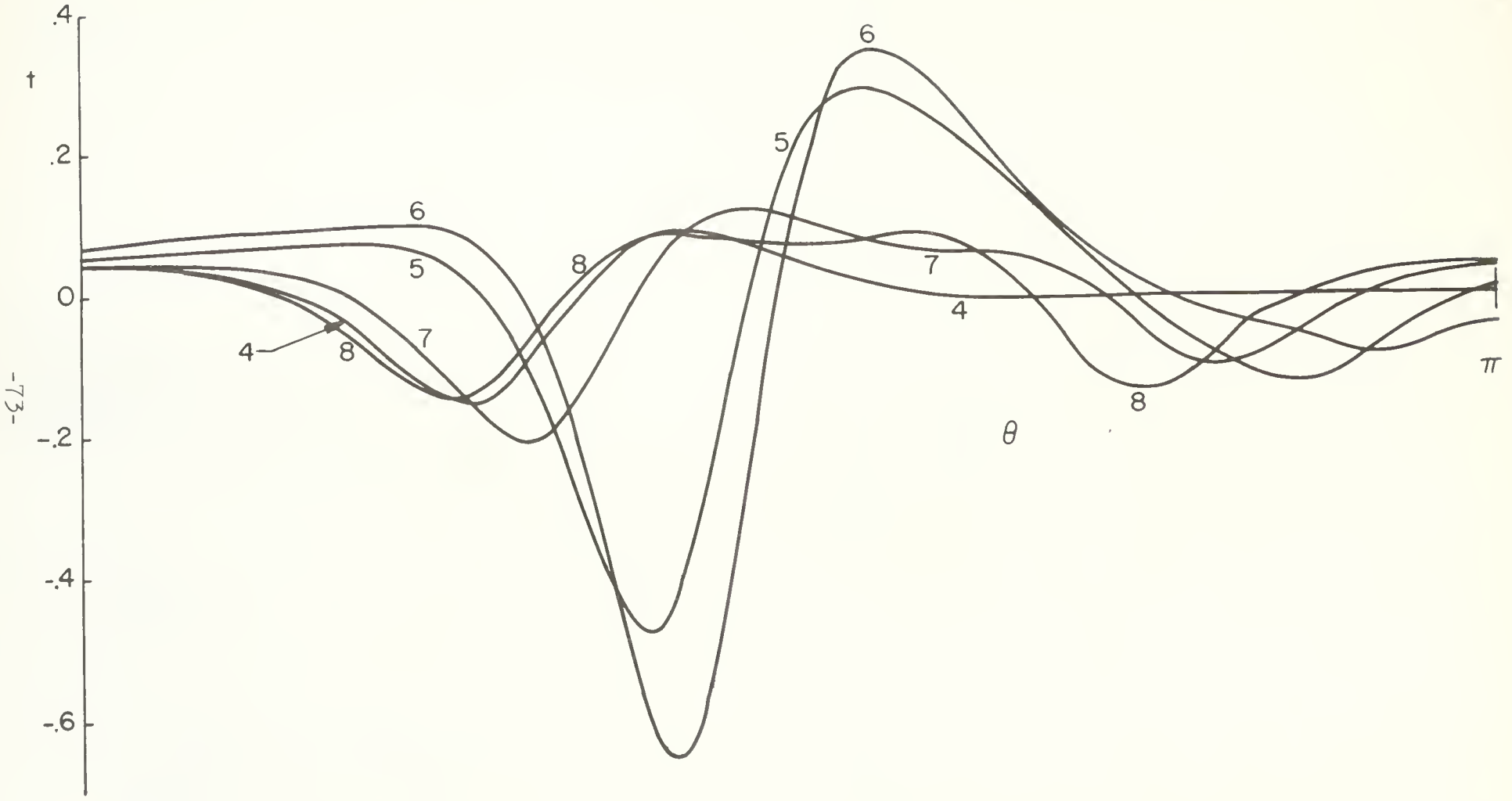
.4
t
.2
0
-.2
-.4
-.6
6
5
8
7
4
θ
π

Figure 9

Graph of P vs. A for the solution branching from P_{16}, the lowest symmetric eigenvalue of the thin sphere.

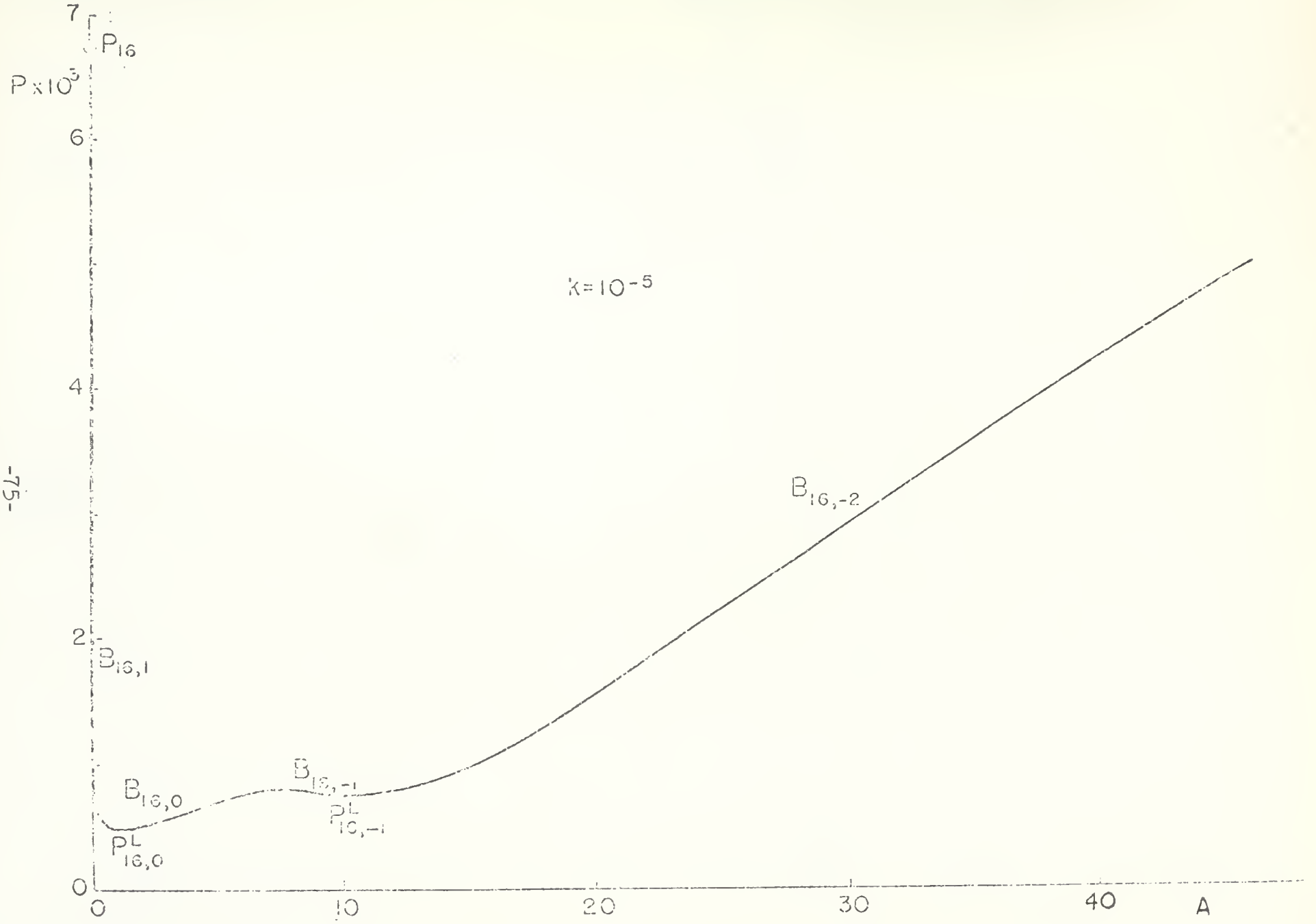
7
P_{16}
$P \times 10^5$
6
$k=10^{-5}$
4
$B_{16,-2}$
2
$B_{16,1}$
$B_{16,0}$
$B_{16,-1}$
$P^L_{16,-1}$
$P^L_{16,0}$
0
0
10
20
30
40
A

Figure 10a

Graphs of $(e/2)^{1/3}$ vs. P for the thin sphere, $k = 10^{-5}$, for the solutions branching from the lowest 5 symmetric eigenvalues. As in Figure 2a, the P axis is horizontal and the circles on the P axis indicate the eigenvalues. Some of the branches and critical loads are labeled. The branch $B_{16,1}$ is not completely shown in the figure. It is shown in Figure 10b.

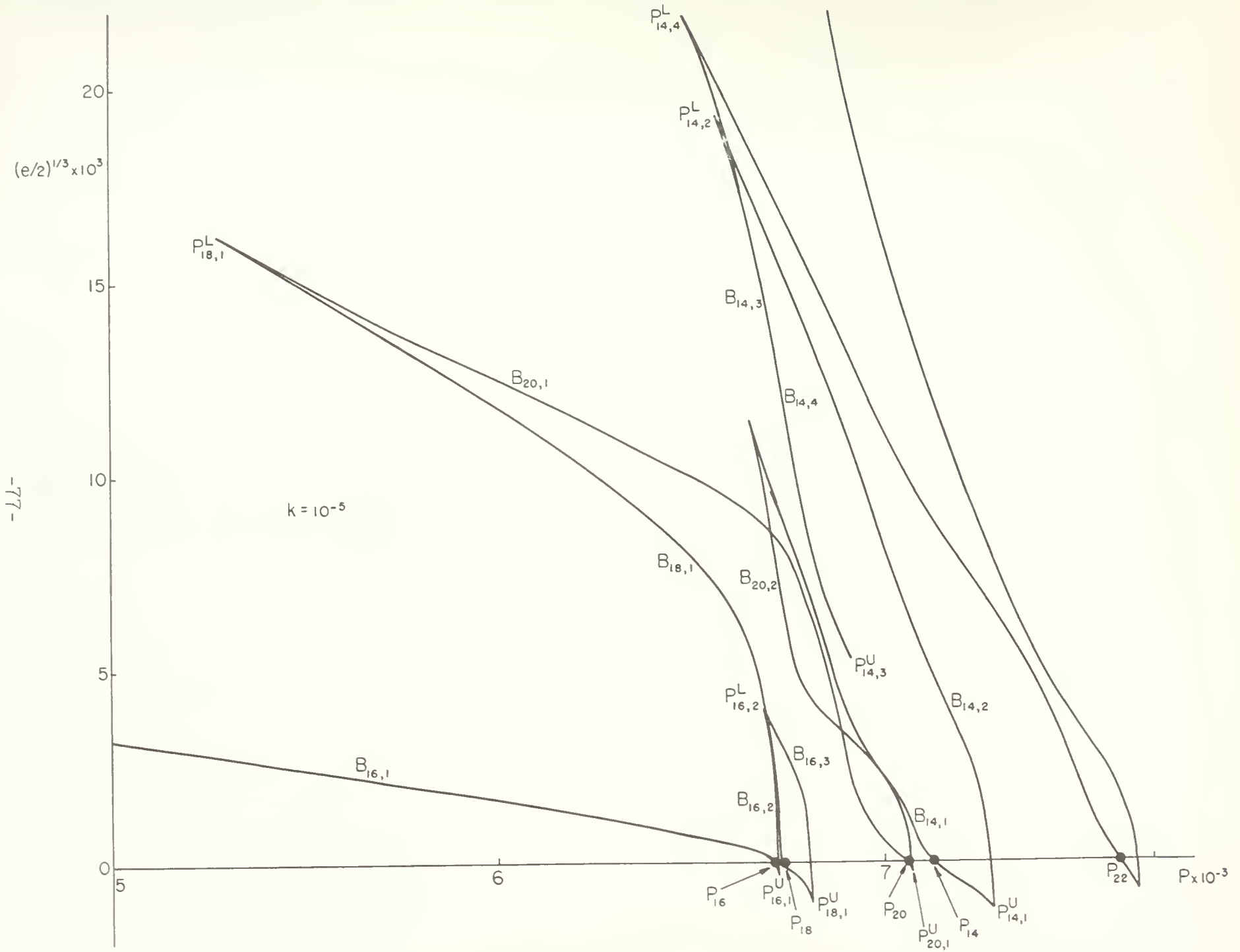
$(e/2)^{1/3} \times 10^3$
20
15
10
5
0
5
6
7
$P \times 10^{-3}$
$k = 10^{-5}$
$P^L_{14,4}$
$P^L_{14,2}$
$P^L_{18,1}$
$B_{20,1}$
$B_{14,3}$
$B_{14,4}$
$B_{18,1}$
$B_{20,2}$
$P^U_{14,3}$
$P^L_{16,2}$
$B_{14,2}$
$B_{16,3}$
$B_{16,1}$
$B_{16,2}$
$B_{14,1}$
P_{16}
$P^U_{16,1}$
$P^U_{18,1}$
P_{18}
P_{20}
$P^U_{20,1}$
P_{14}
$P^U_{14,1}$
P_{22}

Figure 10b

Graphs of $(e/2)^{1/3}$ vs. P for the lower part of $B_{16,1}$ and for the branches $B_{16,0}$, $B_{16,-1}$ and a part of $B_{16,-2}$.

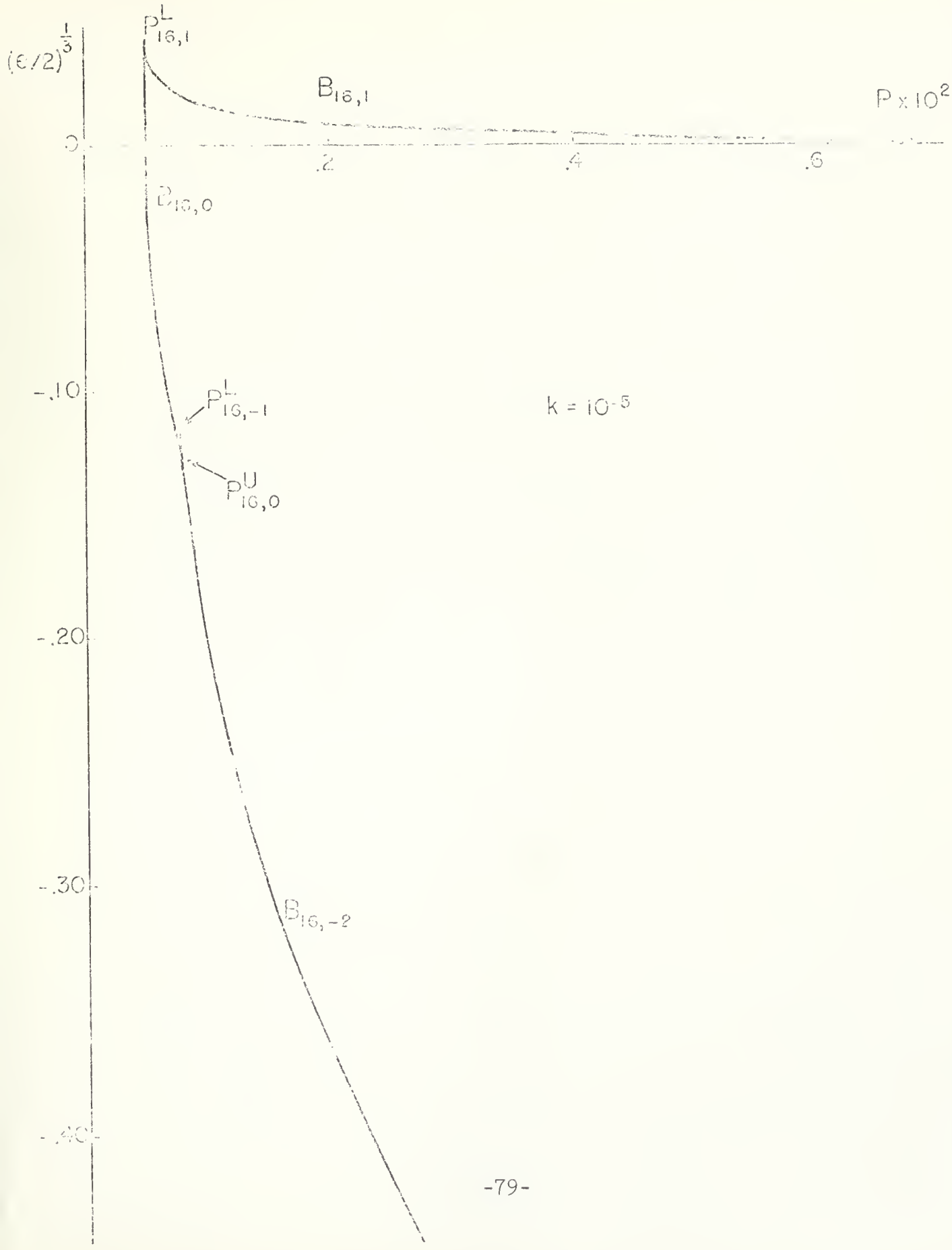
$P^L_{16,1}$
$(\epsilon/2)^{\frac{1}{3}}$
$B_{16,1}$
$P \times 10^2$
0
.2
.4
.6
$P_{16,0}$
-.10
$P^L_{16,-1}$
$k = 10^{-5}$
$P^U_{16,0}$
-.20
-.30
$B_{16,-2}$
-.40

Figure 11

A sketch indicating the local behavior near the lowest eigenvalues for the sphere with $k = 1.2 \times 10^{-5}$. The numerical values for the critical pressures are $P_{16} \doteq .0073217$, $P^{U}_{16,1} = P^{U}_{16,2} \doteq .0073567$, $P^{E}_{16,2} \doteq .0073552$, $P_{17} \doteq .0073640$, $P_{15} \doteq .007392$.

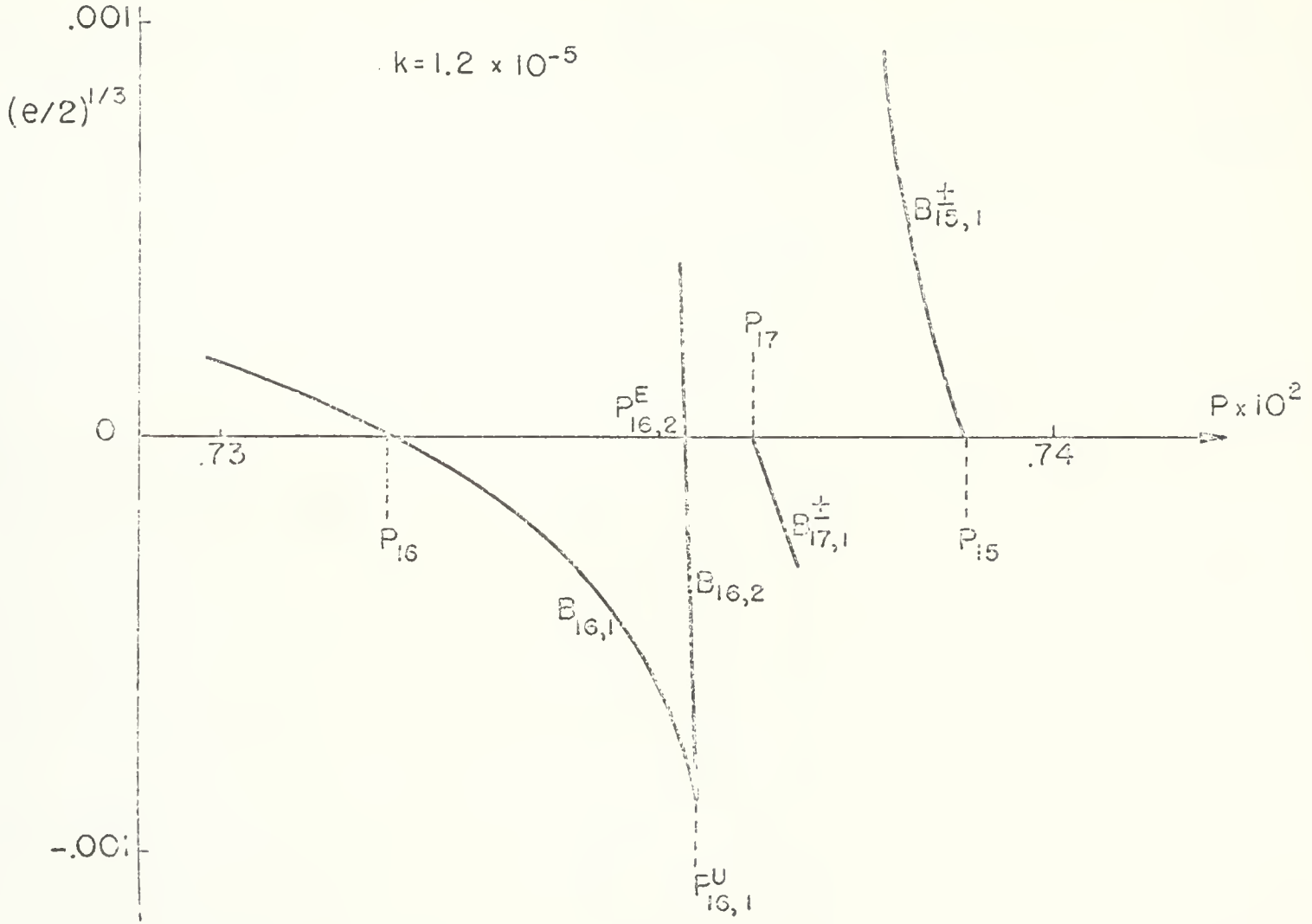
.001
(e/2)^1/3
k = 1.2 x 10^-5
0
-.001
.73
.74
P x 10^2
P16
P17
P15
P^E 16,2
B16,1
B16,2
B^± 17,1
B^± 15,1
P^U 16,1

Figure 12

Graphs of $W(\theta)$ for $P = 6 \times 10^{-4}$ and a sequence of values of k decreasing from $k = 10^{-5}$ (the thin sphere) to $k = 2 \times 10^{-6}$. For $k = 10^{-5}$ the solution corresponds to a point on $B_{16,1}$. The values of $k \times 10^{5}$ are 1, .8, .6, .4, and .2 for the graphs numbered 1 through 5 in that order.

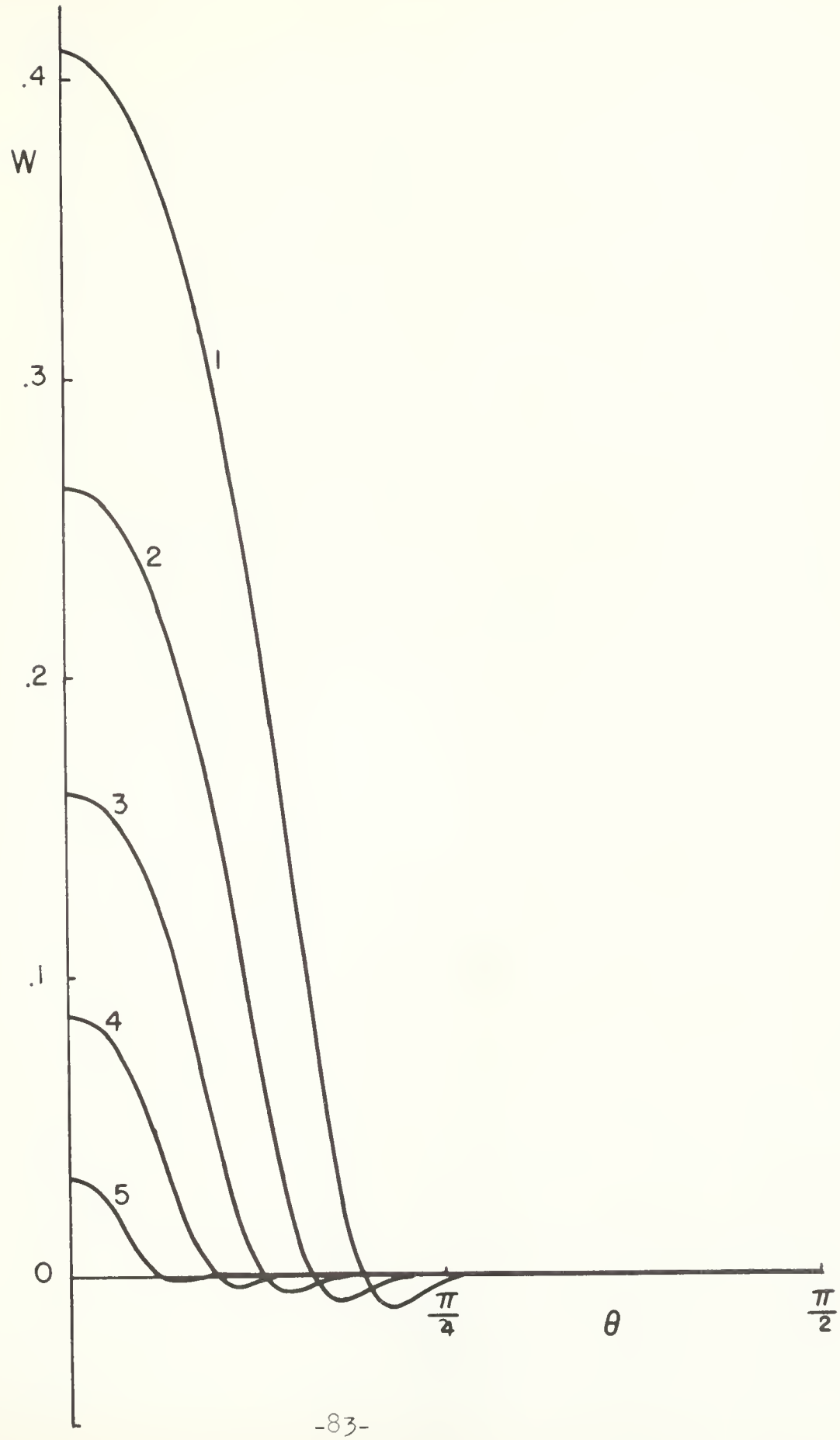
.4
W
.3
.2
.1
0
1
2
3
4
5
π/4
θ
π/2

Figure 13

Graphs of $t(\theta)$ for $P = 6 \times 10^{-4}$ and the same sequence of values of k as in Figure 12.

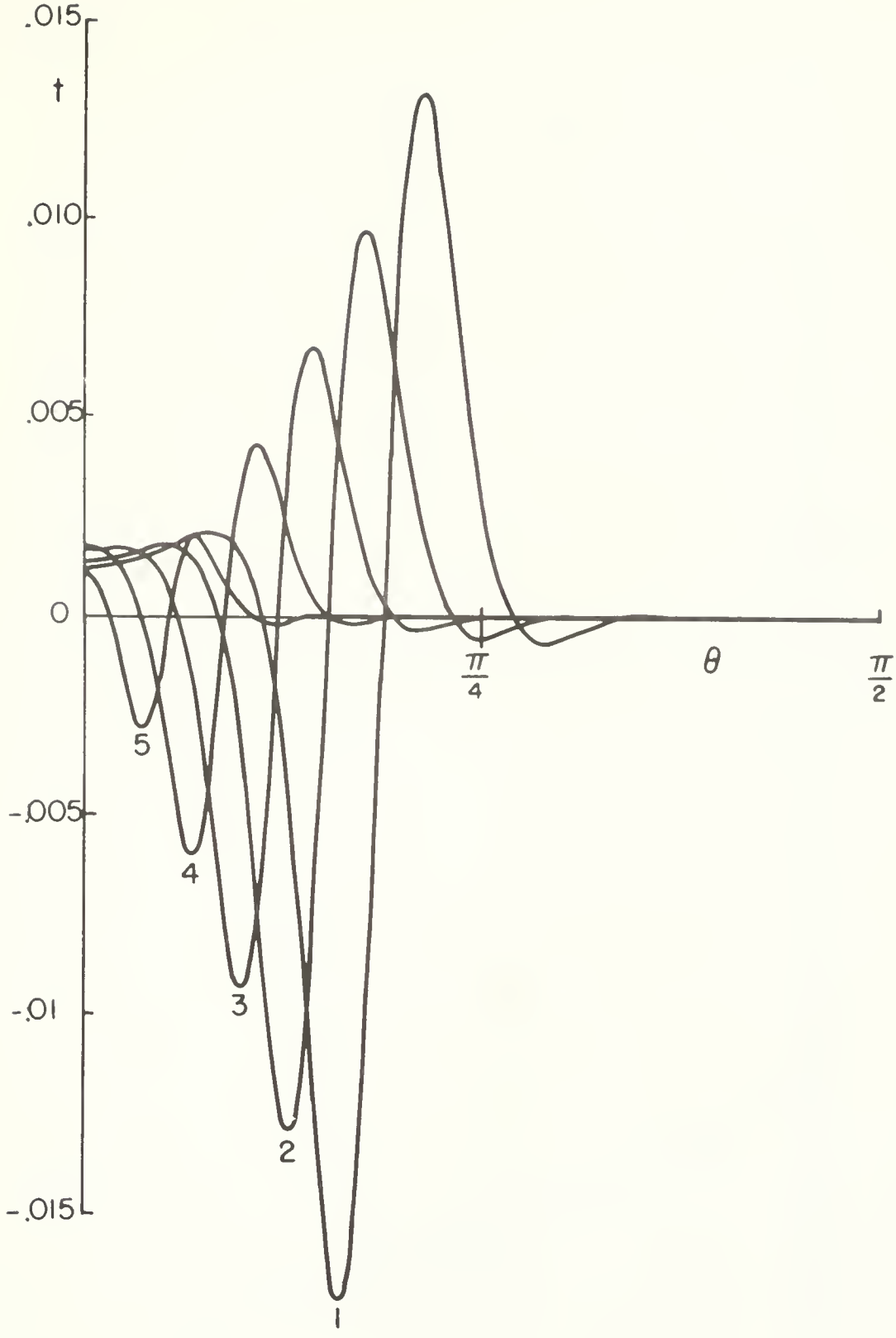
.015
t
.010
.005
0
-.005
-.01
-.015
π/4
θ
π/2
1
2
3
4
5

Figure 14a

Graphs of $W(\theta)$ for two of the 16 solutions at P = .01996 for the thick sphere. Two other solutions are shown in Figure 14b. The remaining solutions are not shown since they differ little from the first solution shown in Figure 14b.

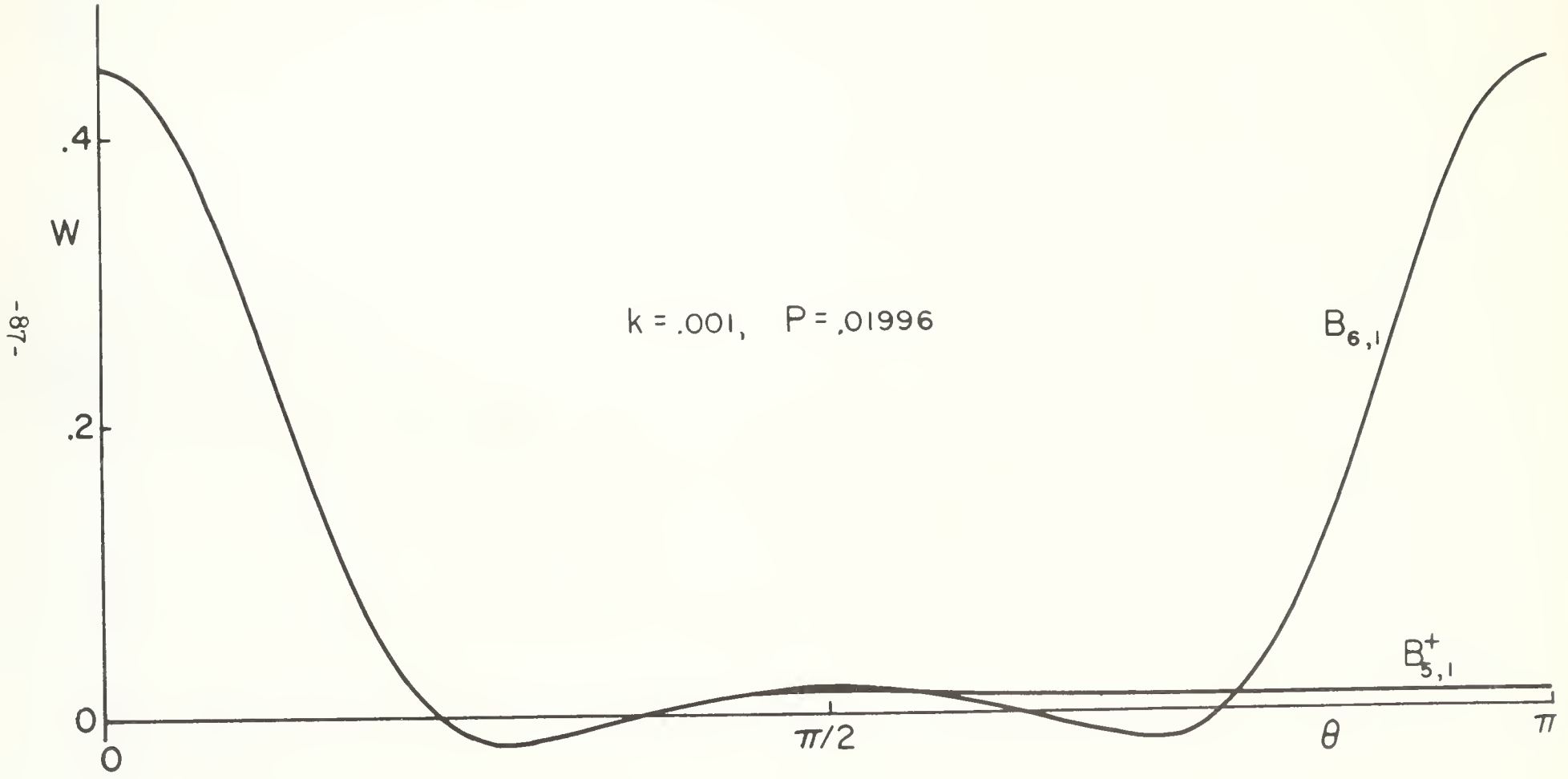
.4
W
.2
0
0
k = .001, P = .01996
$B_{6,1}$
$B^{+}_{5,1}$
$\pi/2$
θ
π

Figure 14b

Graphs of $W(\theta)$ for two of the 16 solutions at P = .01996.

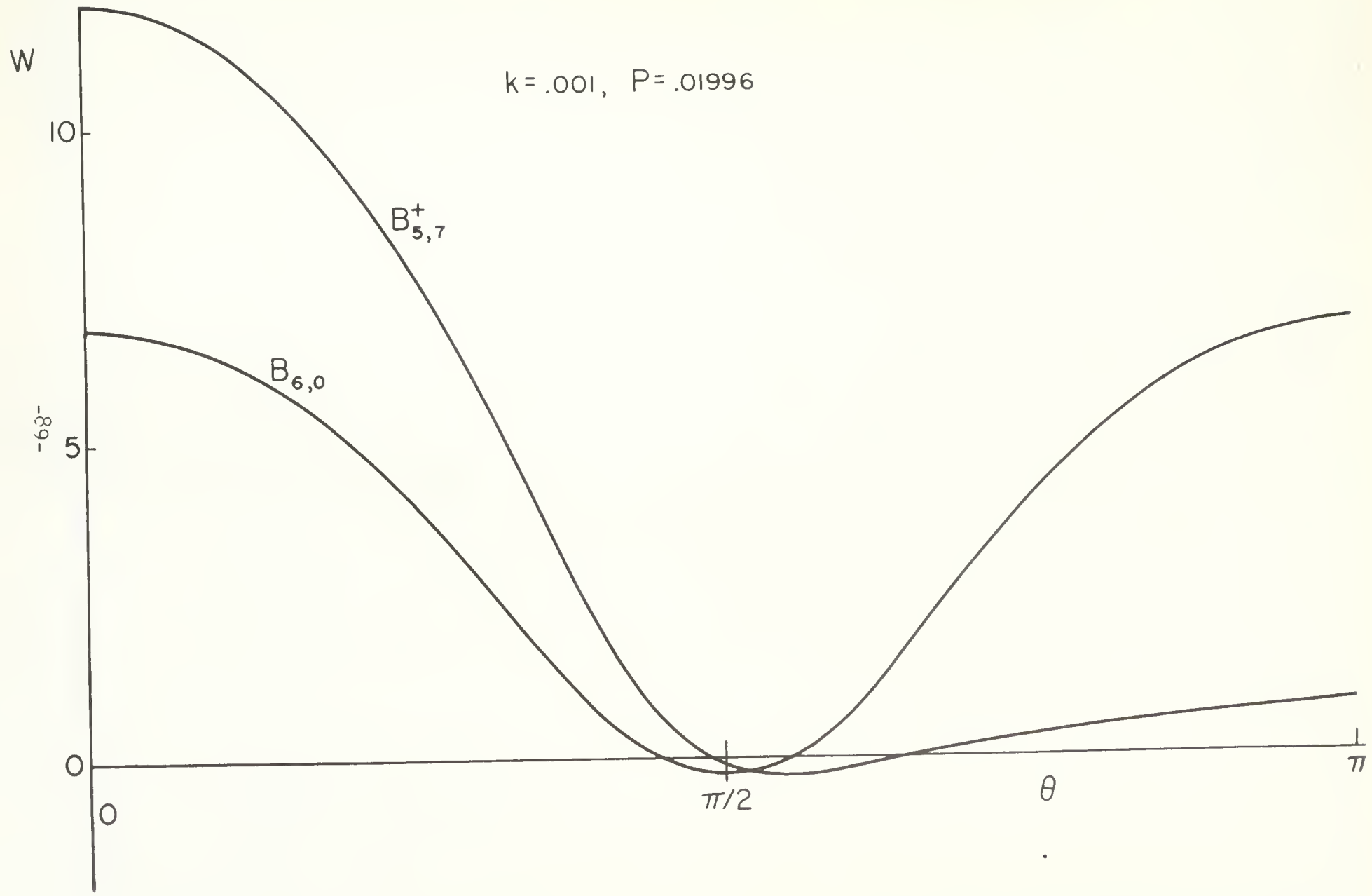
W
k = .001, P = .01996
10
5
0
0
$B^{+}_{5,7}$
$B_{6,0}$
$\pi/2$
θ
π

Security Classification

DOCUMENT CONTROL DATA - R & D

Security classification of title, body of abstract and indexing annotation must be entered when the overall report is classified)

1 ORIGINATING ACTIVITY (Corporate author)	2a. REPORT SECURITY CLASSIFICATION
New York University Courant Institute of Mathematical Sciences	not classified
	2b. GROUP none

3 REPORT TITLE

AXISYMMETRIC BUCKLING OF HOLLOW SPHERES AND HEMISPHERES

4 DESCRIPTIVE NOTES (Type of report and inclusive dates)

Technical Report December 1969

5. AUTHOR(S) (First name, middle initial, last name)

Louis Bauer, Edward L. Reiss and Herbert B. Keller

6. REPORT DATE	7a. TOTAL NO. OF PAGES	7b. NO OF REFS
December 1969	89	15

8a. CONTRACT OR GRANT NO.	9a. ORIGINATOR'S REPORT NUMBER(S)
N00014-67-A-0467-0008	IMM 379
b. PROJECT NO. NR 064-438	
c.	9b. OTHER REPORT NO(S) (Any other numbers that may be assigned this report) (NYO-1480-132)
d.	

10. DISTRIBUTION STATEMENT

Distribution of this document is unlimited.

11. SUPPLEMENTARY NOTES	12. SPONSORING MILITARY ACTIVITY
none	U.S. Navy, Office of Naval Research 207 West 24th St., New York, N.Y.

13. ABSTRACT

A nonlinear thin shell theory is derived for the axisymmetric buckling of spherical shells subjected to either a pressure or a centrally directed surface load. The theory is reduced to a boundary value problem for a system of four first order ordinary differential equations. Numerical solutions of this boundary value problem are obtained by the shooting and parallel shooting methods. An extensive numerical study is made of the nonlinear deformations of the shells. We find for example, that all solution branches that bifurcate from the eigenvalues of the linearized buckling theory are connected to each other by means of intermediate branches. Some implications of the numerical results concerning the buckling of spherical shells are discussed.

DD FORM 1 NOV 65 1473 (PAGE 1)

S/N 0102-014-6600

Security Classification

14 KEY WOROS	LINK A		LINK B		LINK C	
	ROLE	WT	ROLE	WT	ROLE	WT

DISTRIBUTION LIST N00014-67-A-0467-0008

PART I - GOVERNMENT

Administrative & Liaison Activities

Chief of Naval Research
Attn:
Code 423
439 (2)
468
Department of the Navy
Washington, D.C. 20360

Commanding Officer
ONR Branch Office
495 Summer Street
Boston, Massachusetts 02210

Commanding Officer
ONR Branch Office
219 S. Dearborn Street
Chicago, Illinois 60604

New York Area Office
Scientific Department
Office of Naval Research
207 West 24th Street
New York, New York 10011

Commanding Officer
ONR Branch Office
1030 E. Green Street
Pasadena, California 91101

U.S. Naval Research Laboratory
Attn: Technical Information Div. (6)
Washington, D.C. 20390

Defense Documentation Center
Cameron Station (20)
Alexandria, Virginia 22314

Army

Commanding Officer
U.S. Army Research Off. - Durham
Attn: Mr. J.J. Murray
CRD-AA-IP
Box CM, Duke Station
Durham, North Carolina 27706

Commanding Officer
AMXMR-ATL
U.S. Army Materials Res. Agcy.
Watertown, Massachusetts 02172

Redstone Scientific Info. Center
Chief, Document Section
U.S. Army Missile Command
Redstone Arsenal, Alabama 35809

AMSMI-RKP
Attn: Mr. T.H. Duerr
Redstone Arsenal, Alabama 35809

Ballistic Research Laboratories
Attn: Dr. A.S. Elder
Aberdeen Proving Ground
Aberdeen, Maryland 21005

Technical Library
Aberdeen Proving Ground
Aberdeen, Maryland 21005

Navy

Commanding Officer and Director
Attn: Code 042 (Cent. Lib. Br.)
050
700 (Struc. Mech. Lab.)
720
725
740 (Mr. W.J. Sette)
901 (Dr. M. Strassberg)
941 (Dr. R. Liebowitz)
945 (Mr. A.O. Sykes)
960 (Mr. E.F. Noonan)
962 (Dr. E. Buchmann)
David Taylor Model Basin
Washington, D.C. 20007

Mr. Garet A. Bornstein
U.S. Naval Propellant Plant
Indian Head, Maryland 20640

Undersea Explosion Research Div.
Attn: Mr. D.S. Cohen
Code 780
David Taylor Model Basin
Norfolk Naval Shipyard
Portsmouth, Virginia 23709

Commanding Officer & Director
Code 257, Library
U.S. Navy Marine Engr. Lab.
Annapolis, Maryland 21402

Commander
Technical Library
U.S. Naval Ordnance Test Station
Pasadena Annex
3202 E. Foothill Blvd.
Pasadena, California 91107

U.S. Naval Ordnance Test Station
Attn: Dr. Arnold Adicoff
Code 5056
China Lake, California 93557

Commander
U.S. Naval Ordnance Test Station
Mechanical Engineering Division
Code 556
China Lake, California 93557

Commanding Officer & Director
U.S. Naval Civil Engr. Lab.
Code L31
Port Hueneme, California 93041

Shipyard Technical Library
Code 242L
Portsmouth Naval Shipyard
Portsmouth, New Hampshire 03804

U.S. Naval Electronics Laboratory
Attn: Dr. R.J. Christensen
San Diego, California 92152

U.S. Naval Ordnance Laboratory
Mechanics Division
RFD 1, White Oak
Silver Spring, Maryland 20910

U.S. Naval Ordnance Laboratory
Attn: Mr. H.A. Perry, Jr.
Non-Metallic Materials Division
Silver Spring, Maryland 20910

Supervisor of Shipbuilding
U.S. Navy
Newport News, Virginia 23607

Shipyard Technical Library
Building 746, Code 303TL
Mare Island Naval Shipyard
Vallejo, California 94592

Director
U.S. Navy Underwater Sound Ref. Lab.
Office of Naval Research
P.O. Box 8337
Orlando, Florida 32806

Technical Library
U.S. Naval Propellant Plant
Indian Head, Maryland 20640

U.S. Naval Propellant Plant
Attn: Dr. J.G. Tuono
Research & Development Division
Indian Head, Maryland 20640

Chief of Naval Operations
Attn: Code Op-03EG
Op-07T
Department of the Navy
Washington, D.C. 20350

Director, Special Projects
Attn: Sp-001
43
2731
Department of the Navy
Washington, D.C. 20360

Executive Secretary PLRRD
Special Projects Office (Sp-00110)
Department of the Navy
Washington, D.C. 20360

U.S. Naval Applied Science Lab.
Code 9832
Technical Library
Building 291, Naval Base
Brooklyn, New York 11251

Director
Aeronautical Materials Lab.
Naval Air Engineering Center
Naval Base
Philadelphia, Pennsylvania 19112

Navy (Cont.)

Director
Aeronautical Structures Lab.
Naval Air Engineering Center
Naval Base
Philadelphia, Pennsylvania 19112

Director
Attn: Code 5360
5500
6200
6210
6250
6260
Technical Library
Naval Research Laboratory
Washington, D.C. 20390

Chief, Bureau of Naval Weapons
Attn: Code DLI-3
R-12
RAAD-2
RAAD-24 (Mr. E.M. Ryan)
RM
RMMP-2
RMMP-11 (Mr. I. Silver)
RMMP-22 (Mr. J.C. Ardinger)
RR
RRRE
RRRE-61 (Mr. W.J. Marciniak)
RU
Department of the Navy
Washington, D.C. 20360

Chief, Bureau of Ships
Attn: Code 210-L
305
345
421
423
430
440
442
443
1500
Department of the Navy
Washington, D.C. 20360

Commander
U.S. Naval Weapons Laboratory
Dahlgren, Virginia 22448

Mr. Ernest A. Hogge
Head, Scientific Support Division
U.S. Navy Mine Defense Laboratory
Panama City, Florida 32402

Bureau of Yards & Docks Tech. Lib.
Yards & Docks Annex
Department of the Navy
Washington, D.C. 20390

Air Force

Commander, WADD
Attn: Code WWRMDD
AFFDL (FDDS)
Structures Division
AFLC (MCEEA)
Code WWRMDS
AFFDL (FDT)
Code WWRC
AFML (MAAM)
Code WCLSY
SEG (SEFSD, Mr. Lakin)
Wright-Patterson Air Force Base
Dayton, Ohio 45433

Commander
Chief, Applied Mechanics Group
U.S. Air Force Inst. of Tech.
Wright-Patterson Air Force Base
Dayton, Ohio 45433

Chief, Civil Engineering Branch
WLRC, Research Division
Air Force Weapons Laboratory
Kirtland AFB, New Mexico 87117

Commander
AFRPL (RPMC/Dr. F.N. Kelley)
Edwards AFB, California 93523

Commander
Attn: Mr. A.L. Skinner, OOMQQC
Hill AFB, Utah 84401

Commander
Mechanics Division
Air Force Office of Scien. Res.
Washington, D.C. 20333

NASA

Structures Research Division
Attn: Mr. R.R. Heldenfels, Chief
National Aeronautics & Space Admin.
Langley Research Center
Langley Station
Hampton, Virginia 23365

NASA (cont'd.)

National Aeronautics & Space Admin.
Code RV-2
Washington, D.C. 20546

National Aeronautics & Space Admin.
Associate Administrator for Advanced
Research & Technology
Washington, D.C. 20546

Scientific & Tech. Info. Facility
NASA Representative (S-AK/DL)
P.O. Box 5700
Bethesda, Maryland 20014

Other Government Activities

Commandant
Chief, Testing & Development Div.
U.S. Coast Guard
1300 E Street, N.W.
Washington, D.C. 20226

Director
Marine Corps Landing Force Devel. Cen.
Marine Corps Schools
Quantico, Virginia 22134

Director
Attn: Mr. B.L. Wilson
National Bureau of Standards
Washington, D.C. 20234

National Science Foundation
Engineering Division
1951 Constitution Avenue, N.W.
Washington, D.C. 20550

Science & Tech. Division
Library of Congress
Washington, D.C. 20540

Director
STBS
Defense Atomic Support Agency
Washington, D.C. 20301

Commander Field Command
Defense Atomic Support Agency
Sandia Base
Albuquerque, New Mexico 87115

Chief, Defense Atomic Support Agcy.
Blast & Shock Division
The Pentagon
Washington, D.C. 20301

Director Defense Research & Engr.
Technical Library
Room 3C-128
The Pentagon
Washington, D.C. 20301

Chief, Airframe & Equipment Branch
FS-120
Office of Flight Standards
Federal Aviation Agency
Washington, D.C. 20553

Chief, Division of Ship Design
Maritime Administration
Washington, D.C. 20235

Deputy Chief, Office of Ship Constr.
Attn: Mr. U.L. Russo
Maritime Administration
Washington, D.C. 20235

Executive Secretary
Committee on Undersea Warfare
National Academy of Sciences
2101 Constitution Avenue
Washington, D.C. 20418

Ship Hull Research Committee
Attn: Mr. A.R. Lytle
National Research Council
National Academy of Sciences
2101 Constitution Avenue
Washington, D.C. 20418

PART II - CONTRACTORS AND OTHER
TECHNICAL COLLABORATORS

Universities

Dr. D.C. Drucker
Division of Engineering
Brown University
Providence, Rhode Island 02912

Professor J. Edmund Fitzgerald
Chairman, Department of Civil
Engineering
University of Utah
Salt Lake City, Utah 84112

Universities (cont'd.)

Prof. M. E. Gurtin
Department of Mathematics
Carnegie Institute of Technology
Pittsburgh, Pennsylvania 15213

Prof. R.S. Rivlin
Center for Application of Mathematics
Lehigh University
Bethlehem, Pennsylvania 18015

Prof. P.J. Blatz
Materials Science Department
California Institute of Technology
Pasadena, California 91109

Prof. Julius Miklowitz
Div. of Engr. & Applied Sciences
California Institute of Technology
Pasadena, California 91109

Prof. George Sih
Department of Mechanics
Lehigh University
Bethlehem, Pennsylvania 18015

Solid Propellant Library
Firestone Flight Science Lab.
California Institute of Technology
Pasadena, California 91109

Prof. Eli Sternberg
Div. of Engr. & Applied Sciences
California Institute of Technology
Pasadena, California 91109

Prof. Paul M. Naghdi
Div. of Applied Mechanics
Etcheverry Hall
University of California
Berkeley, California 94720

Prof. J. Baltrukonis
Mechanics Division
The Catholic Univ. of America
Washington, D.C. 20017

Dr. Y. Weitsman
Div. of Applied Mathematics
Brown University
Providence, Rhode Island 02912

Prof. A.J. Durelli
Mechanics Division
The Catholic Univ. of America
Washington, D. C. 20017

Prof. H.H. Bleich
Department of Civil Engr.
Columbia University
Amsterdam & 120th Street
New York, New York 10027

Prof. R.D. Mindlin
Department of Civil Engr.
Columbia University
S.W. Mudd Building
New York, New York 10027

Prof. B.A. Boley
Department of Civil Engr.
Columbia University
Amsterdam & 120th Street
New York, New York 10027

Prof. F.L. DiMaggio
Department of Civil Engr.
Columbia University
616 Mudd Building
New York, New York 10027

Prof. William A. Nash
Dept. of Mechanical and Aerospace Engineering
College of Engineering
University of Massachusetts
Amherst, Massachusetts 01002

Prof. B. Budiansky
Div. of Engr. & Applied Physics
Pierce Hall
Harvard University
Cambridge, Massachusetts 02138

Prof. P.G. Hodge
Department of Mechanics
Illinois Institute of Technology
Chicago, Illinois 60616

Dr. S. Dharmarajan
Head, Post Graduate Dept. of Machine Design & Mechanics
P.S.G. College of Technology
Coimbatore, Madras State
India

Prof. A.M. Freudenthal
Dept. of Civil Engr. & Engr. Mech.
Columbia University
New York, New York 10027

Universities (Cont'd)

Prof. H.T. Corten
321 Talbot Lab.
University of Illinois
Urbana, Illinois 61803

Prof. W.J. Hall
Department of Civil Engr.
University of Illinois
Urbana, Illinois 61803

Prof. N.M. Newmark
Dept. of Civil Engineering
University of Illinois
Urbana, Illinois 61803

Dr. W.H. Avery
Applied Physics Laboratory
Johns Hopkins University
8621 Georgia Avenue
Silver Spring, Maryland 20910

Prof. J.B. Tiedemann
Dept. of Aero. Engr. & Arch.
University of Kansas
Lawrence, Kansas 66045

Prof. S. Taira
Department of Engineering
Kyoto University
Kyoto, Japan

Prof. E. Reissner
Dept. of Mathematics
Massachusetts Inst. of Tech.
Cambridge, Massachusetts 02139

Library (Code 0384)
U.S. Naval Postgraduate School
Monterey, California 93940

Dr. Joseph Marin
Prof. of Materials Science
Dept. of Materials Sc. & Chem.
U.S. Naval Postgraduate School
Monterey, California 93940

Prof. E.L. Reiss
Courant Inst. of Math. Sciences
New York University
251 Mercer Street
New York, New York 10012

Dr. Francis Cozzarelli
Div. of Interdisciplinary
Studies and Research
School of Engineering
State Univ. of N.Y. at Buffalo
Buffalo, New York 14214

Dr. George Herrmann
The Technological Institute
Northwestern University
Evanston, Illinois 60201

Director, Ordnance Research Lab.
The Pennsylvania State University
P.O. Box 30
State College, Pennsylvania 16801

Dean Oscar Baguio
College of Engineering
University of the Philippines
Quezon City, Philippines

Prof. J. Kempner
Dept. of Aero. Engr. & Applied Mech.
Polytechnic Institute of Brooklyn
333 Jay Street
Brooklyn, New York 11201

Prof. Jl Klosner
Polytechnic Institute of Brooklyn
333 Jay Street
Brooklyn, New York 11201

Prof. F. R. Eirich
Polytechnic Institute of Brooklyn
333 Jay Street
Brooklyn, New York 11201

Prof. A. Eringen
Aerospace & Mechanical Sciences
Princeton University
Princeton, New Jersey

Tamar Singer
Library of Exact Science
Tel Aviv University
Ramat Aviv, Tel Aviv, Israel

Prof. Eugen J. Skudrzyk
Department of Physics
Ordnance Research Lab.
The Pennsylvania State University
P. O. Box 30
State College, Pennsylvania 16801

Universities (cont'd.)

Dr. S.L. Koh
School of Aero., Astro. & Engr. Sc.
Purdue University
Lafayette, Indiana 47907

Prof. D. Schapery
Purdue University
Lafayette, Indiana 47907

Prof. E.H. Lee
Div. of Engr. Mechanics
Stanford University
Stanford, California 94305

Dr. Nicholas J. Hoff
Dept. of Aero. & Astro.
Stanford University
Stanford, California 94305

Prof. J.N. Goodier
Div. of Engr. Mechanics
Stanford University
Stanford, California 94305

Prof. Markus Reiner
Technion R & D Foundation, Ltd.
Haifa, Israel

Prof. Tsuyoshi Hayashi
Department of Aeronautics
Faculty of Engineering
University of Tokyo
BUNKYO-KU
Tokyo, Japan

Prof. R.J.H. Bollard
Chairman, Aeronautical Engr. Dept.
207 Guggenheim Hall
University of Washington
Seattle, Washington 98105

Prof. Albert S. Kobayashi
Dept. of Mechanical Engr.
University of Washington
Seattle, Washington 98105

Officer-in-Charge
Post Graduate School for Naval Off.
Webb Institute of Naval Arch.
Crescent Beach Road, Glen Cove
Long Island, New York 11542

Industry and Research Institutes

Mr. K.W. Bills, Jr.
Dept. 4722, Bldg. 0525
Aerojet-General Corporation
P.O. Box 1947
Sacramento, California 95809

Dr. James H. Wiegand
Senior Dept. 4720, Bldg. 0525
Ballistics & Mech. Properties Lab.
Aerojet-General Corporation
P.O. Box 1947
Sacramento, California 95809

Mr. J.S. Wise
Aerospace Corporation
P.O. Box 1308
San Bernardino, California 92402

Dr. Vito Salerno
Applied Technology Assoc., Inc.
29 Church Street
Ramsey, New Jersey 07446

Library Services Department
Report Section, Bldg. 14-14
Argonne National Laboratory
9700 S. Cass Avenue
Argonne, Illinois 60440

Dr. E. M. Kerwin
Bolt, Beranek, & Newman, Inc.
50 Moulton Street
Cambridge, Massachusetts 02138

Dr. M. C. Junger
Cambridge Acoustical Associates
129 Mount Auburn Street
Cambridge, Massachusetts 02138

Dr. F.R. Schwarzl
Central Laboratory T.N.O.
134 Julianalaan
Delft, Holland

Industry & Research Inst. (cont'd.)

Mr. Ronald D. Brown
Applied Physics Laboratory
Chemical Propulsion Agency
8621 Georgia Avenue
Silver Spring, Maryland 20910

Research and Development
Electric Boat Division
General Dynamics Corporation
Groton, Connecticut 06340

Supervisor of Shipbuilding, USN,
and Naval Insp. of Ordnance
Electric Boat Division
General Dynamics Corporation
Groton, Connecticut 06340

Dr. L.H. Chen
Basic Engineering
Electric Boat Division
General Dynamics Corporation
Groton, Connecticut 06340

Mr. Ross H. Petty
Technical Librarian
Allegany Ballistics Lab.
Hercules Powder Company
P.O. Box 210
Cumberland, Maryland 21501

Dr. J.H. Thacher
Allegany Ballistic Laboratory
Hercules Powder Company
Cumberland, Maryland 21501

Dr. Joshua E. Greenspon
J. G. Engr. Research Associates
3831 Menlo Drive
Baltimore, Maryland 21215

Mr. R.F. Landel
Jet Propulsion Laboratory
4800 Oak Grove Drive
Pasadena, California 91103

Mr. G. Lewis
Jet Propulsion Laboratory
4800 Oak Grove Drive
Pasadena, California 91103

Library
Newport News Shipbuilding &
Dry Dock Company
Newport News, Virginia 23607

Mr. E.A. Alexander (Research Dept. 991)
Rocketdyne Division
North American Aviation, Inc.
6633 Canoga Avenue
Canoga Park, California 91304

Mr. Cezar P. Nuguid
Deputy Commissioner
Philippine Atomic Energy Commission
Manila, Philippines

Mr. S.C. Britton
Solid Rocket Division
Rocketdyne
P.O. Box 548
McGregor, Texas 76657

Dr. A.J. Ignatowski
Redstone Arsenal Research Div.
Rohm & Haas Company
Huntsville, Alabama 35807

Dr. M.L. Merritt
Division 5412
Sandia Corporation
Sandia Base
Albuquerque, New Mexico 87115

Director
Ship Research Institute
Ministry of Transportation
700, SHINKAWA
Mitaka
Tokyo, Japan

Dr. H. N. Abramson
Southwest Research Institute
8500 Culebra Road
San Antonio, Texas 78206

Industry and Research Inst. (cont'd.)

Dr. R. C. DeHart
Southwest Research Institute
8500 Culebra Road
San Antonio, Texas 78206

Dr. Thor Smith
Stanford Research Institute
Menlo Park, California 94025

Dr. M. L. Baron
Paul Weidlinger, Consulting Engr.
777 Third Ave. - 22nd Floor
New York, New York 10017

Dr. T. C. Fan
The Rand Corporation
1700 Main Street
Santa Monica, California 90406

Dr. G. R. Makepeace
Director, Research and Engineering
Lockheed Propulsion Company
P.O. Box 111
Redlands, California 92374

Stanford University
Mathematics Department
Stanford, California 94305

Massachussetts Institute of
Technology
Mathematics Department
Room 2-247
Cambridge, Massachussetts 02139

Director, Naval Research Laboratory (5)
Attn: Library
Code 2029(ONRL)
Washington, D.C. 20390

Library (2)
Courant Institute of Mathematical
Sciences
New York University
251 Mercer Street
New York, New York 10012

Science Library
Brown 120
New York University
New York, New York 10012

Office of Naval Research
San Francisco Area Office
50 Fell Street
San Francisco, California 94102

Office of Naval Research (2)
Department of the Navy
(Code 432)
Washington, D.C. 20360